Journal of Geoscience and Environment Protection, 2025, 13(9), 192-223
https://www.scirp.org/journal/gep
ISSN Online: 2327-4344
ISSN Print: 2327-4336

Petrological Characterization of Pyroclastics from the Manengouba Maars Volcanoes, Coastal/Southwest Region, Cameroon

Bibiche Scheila Zemfack Dongmo[1*], Jules Tamen[1], Théophile Njanko[1,2], Paterne Mulimbi Kagarabi[1,3]

[1]Department of Earth Sciences, Faculty of Science, University of Dschang, Dschang, Cameroun
[2]Mnistry of Scientific Research and Innovation, Division for the Utilization and the Extension of the Research Results/Utilization Unit, Yaoundé, Cameroon
[3]Filière de Géologie, Domaine des Sciences et Technologie, Université Officielle de Bukavu, Bukavu, Democratic Republic of the Congo
Email: *Scheilazemfack@gmail.com

How to cite this paper: Zemfack Dongmo, B. S., Tamen, J., Njanko, T., & Mulimbi Kagarabi, P. (2025). Petrological Characterization of Pyroclastics from the Manengouba Maars Volcanoes, Coastal/Southwest Region, Cameroon. *Journal of Geoscience and Environment Protection, 13,* 192-223.
https://doi.org/10.4236/gep.2025.139009

Received: July 27, 2025
Accepted: September 23, 2025
Published: September 26, 2025

Abstract

This study explores the magmatic and eruptive processes of the Manengouba maars, located along the Cameroon Volcanic Line (CVL). Petrographic analyses of the samples reveal a diverse mineralogical composition with clinopyroxenes (20% - 35%), plagioclases (19% - 35%), olivines (5% - 15%), and sanidines (up to 15%). Positive Europium (Eu) anomalies observed suggest crystallization under reducing conditions. X-ray diffraction analyses show a significant presence of smectite (25.99% to 76.05%), kaolinite, and other clay minerals, indicating extensive hydrothermal alteration. Geochemical diagrams reveal clear trends of magmatic fractionation, with an increase in Zr (up to 200 ppm) with increasing SiO_2 (45% to 60%) and a decrease in MgO (from 10% to less than 5%) accompanied by an increase in Nb (from 10 to 50 ppm). These trends suggest magmatic differentiation prior to the eruption. Explosive interactions between ascending magma and groundwater led to phreatomagmatic explosions, forming complex diatremic structures. The presence of mantle xenoliths and host rock fragments indicates significant assimilation of the host rocks during magma ascent, modifying its chemical composition. The results allow proposing a diatreme growth model, highlighting the importance of phreatomagmatic interactions and magmatic fractionation processes. Compared to other volcanic regions, the geology of Manengouba shows significant similarities with other volcanoes along the CVL and with maars and diatremes studied elsewhere in the world. In conclusion, this study enriches our understanding of volcanic and magmatic processes in the Manengouba region, providing crucial insights into eruptive dynamics and associated geochemical and mineralogical conditions.

Keywords

Manengouba Maars, Hydrothermal Alteration, Magmatic Fractionation, Phreatomagmatic Explosions, Diatreme Growth model

1. Introduction

The recognition of pyroclastic deposits, due to their nature, mode of establishment, and tectonic activity, requires petrographic, mineralogical, and geochemical characterization. In the case of monogenetic volcanoes, from a geochemical and volcanological perspective, a high degree of magmatic evolution is observed compared to polygenetic volcanoes (Brenna et al., 2010). Polygenetic eruptions are characterized by a long period of episodic activity. Generally, they occur repeatedly from the same emission site or the same magma chamber (Kereszturi et al., 2013). The presence of different types of rocks, structures, and stratifications in a maar volcano suggests that its emergence occurred over sometimes prolonged periods, often with significant phases of inactivity between volcanic phases (Kereszturi et al., 2013).

Recently, it has become possible to determine the geochemical evolution within pyroclastic deposits while highlighting the compositions and chemical variations in a monogenetic volcano; for example, in the Barombi-Bo maar (Kumba, southwest Cameroon) by Chako Tchamabé et al. (2014) and Kelud volcano, Indonesia by Indriyanto et al. (2023). The presence of lithic rock fragments and heavy minerals (olivine, epidote, and rutile) is an excellent indicator of source rocks (Boggs, 2009). The chemistry of the minerals and the mineralogical composition constituting the pyroclastics are good indicators for understanding their provenance, the alteration of the parent rock, and the tectonic framework of the source area.

In basaltic maar-diatreme volcanoes, vertical migration or mobility of explosion sites occurs when an active vertical hydrological fault is occupied by a dyke feeding a developing volcano, leading to thermo-hydraulic explosions. Vertical or lateral mobility of explosion sites in the root zone controls the growth of the conduit and the distribution of facies within the conduit (Branney & Kokelaar, 2002; Kurszlaukis & Fulop, 2013; Pedrazzi et al., 2013).

Stratigraphic and granulometric studies of the Manengouba maars lead us to think that they have the configuration of polycyclic maars, where each eruptive style occurred from the same diatreme, thus involving lateral or vertical migration of eruptive vents. This work aims to study (1) the composition of the deposits of the Manengouba maars (MM, MF, and MDS). However, since polycyclic activity can be associated with variations in chemical composition, this work also aims to determine whether the magmas that produced these Manengouba maars come from different sources with different compositions or if all eruptive cycles were supported by a single magma chamber, and finally, to understand their

feeding system.

The Manengouba region (Figure 1), located along the Cameroon Volcanic Line (CVL), is a major area of interest for studying volcanic processes due to its diverse magmatic activity (Kagou Dongmo et al., 2001, 2010; Pouclet et al., 2014; Zangmo Tefogoum et al., 2021). The CVL extends over approximately 1600 km, traversing Cameroon and extending into the Atlantic to Bioko Island. This region is characterized by a series of complex volcanoes, including maar-diatremes, which are formed by explosive eruptions when magma comes into contact with groundwater, creating pipe-shaped structures called diatremes (Fitton & Dunlop, 1985; Ngounouno et al., 2001). This study aims to analyze the mineralogical composition of pyroclastic deposits and volcanic rocks from the Manengouba maars to understand the processes of fractional crystallization and alteration. Furthermore, it seeks to assess how deep magmatic sources influence the composition and evolution of the diatremes. Finally, the study uses geochemical and petrographic data to model volcanic processes and propose a growth model for the diatremes in this region.

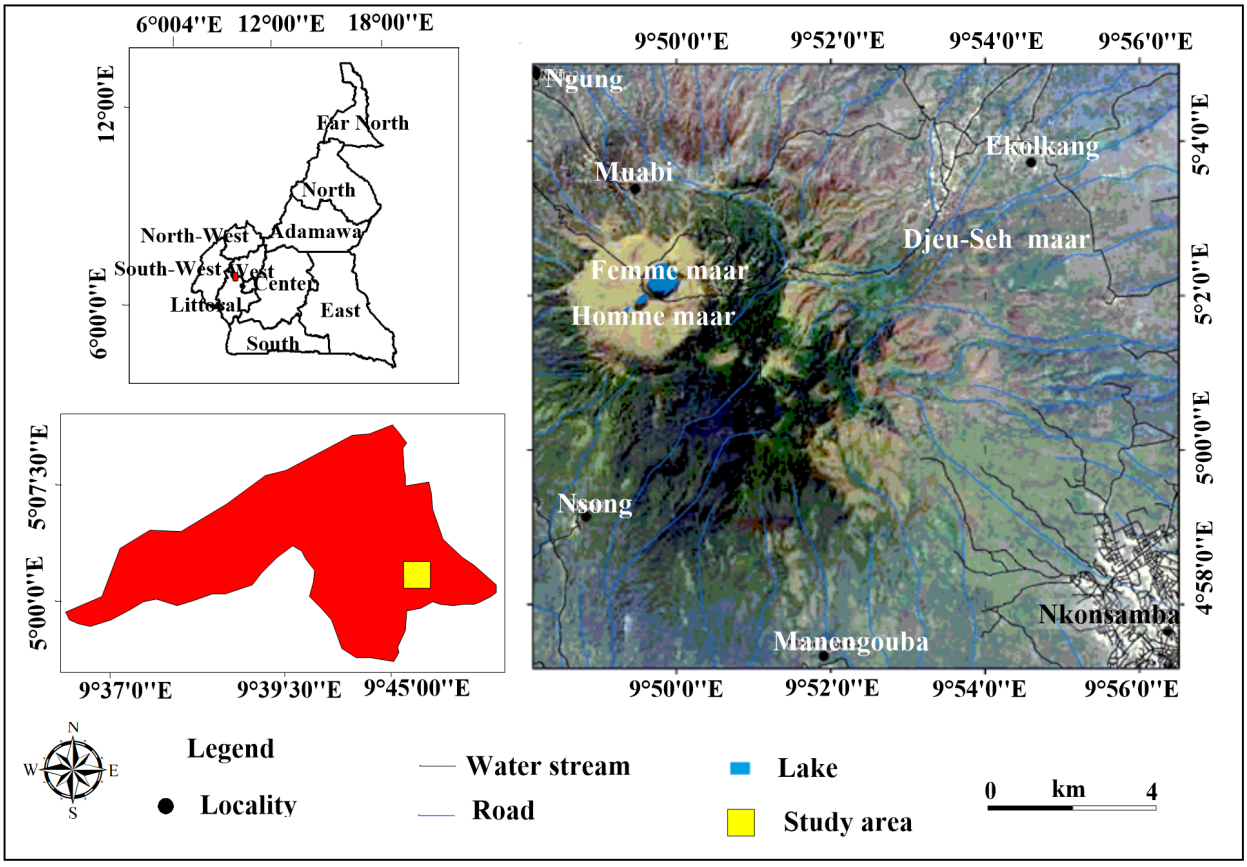

Figure 1. Location map of the Manengouba maars. The two small figures are Cameroon administrative map generated from ArcGIS while the biggest figure is from Google Earth.

Fitton & Dunlop (1985) explored the geochemistry of basalts along the CVL, highlighting the heterogeneity of mantle sources and geochemical variations

along this volcanic line. Ngounouno et al. (2001) analyzed eruptive processes and volcanic products in the Manengouba region, providing a solid basis for studying magma-water interactions and maar formation processes.

To achieve the objectives of this study, we formulated the following research questions: What are the dominant minerals in the pyroclastic deposits, and how does their distribution vary with depth? What specific geochemical anomalies are observed in trace elements (notably REE), and how can they be explained by magmatic processes? How do interactions between magma and groundwater influence the structure and composition of the diatremes?

To answer these questions, we used a combination of field methods, petrographic analyses, and advanced geochemical techniques (Chako Tchamabé et al., 2023). Samples were collected at different depths and sites around the Manengouba maars, and detailed analyses were conducted to determine their mineralogical and chemical composition. Sampling sites were selected based on their geological representativeness and accessibility. Petrographic analyses were performed using optical and electron microscopy to study the textures and compositions of minerals. Geochemical analyses used mass spectrometry (ICP-MS) and X-ray fluorescence (XRF) to determine major and trace element concentrations.

2. Geological Context

2.1. The Cameroon Volcanic Line

The Cameroon Volcanic Line (CVL) is a major geological structure extending approximately 1600 km from the Gulf of Guinea to Lake Chad. This volcanic line traverses Cameroon and includes several active and extinct volcanoes, such as Mount Cameroon, Mount Manengouba, and Mount Oku, as well as volcanic islands like Bioko and Annobón. The CVL is a spectacular manifestation of intraplate magmatic activity, resulting from the upwelling of mantle plumes through the continental lithosphere (Fitton & Dunlop, 1985).

2.2. Tectonic Context

The CVL is situated at the intersection of several tectonic plates, including the African plate and the Cameroon microplate. This region is influenced by complex tectonic forces, including continental rifting associated with the opening of the South Atlantic and the movements of the surrounding tectonic plates. The compressional and tensional forces in this area contribute to the formation of fractures and faults, which facilitate magma's ascent to the surface (Ngounouno et al., 2001).

2.3. Geology of the Manengouba Region

Mount Manengouba (MM) is a volcanic complex located in the center of the Cameroon Volcanic Line (CVL). It covers a total area of ~500 km2 and is set on granito-gneissic basement rocks overlain by Lower Oligocene (30 Ma) (Tchoua, 1974)

basaltic flows featuring the onset of the anorogenic magmatic activity in the area. It is composed of two nested calderas, formed by explosive volcanic eruptions (**Figure 2**). The Manengouba region has a long history of volcanic activity, with eruptions recorded since the Holocene. The erection of the MM was sequenced into either three (Kagou Dongmo et al., 2001) or four successive phases (Pouclet et al., 2014) ranging from the Pleistocene to the Present (1.94 - 0.11 Ma). According to Pouclet et al. (2014), the first phase (1.55 - 0.94 Ma) mainly built the Manengouba shield volcano, whose current boundaries are those of the Elengoum volcano. The second phase (0.94 - 0.89 Ma) resulted in the construction of the stratovolcano of Eboga. The third phase (0.89 - 0.70 Ma) was essentially characterized by tectonic activities, namely the collapse of the upper part yielding the Elengoum and Eboga nested calderas on the one hand, and the extrusions of the syn- to post-caldera felsic domes and needles on the other. The fourth and vanishing phase (0.45 - 0.11 Ma) was marked by effusive and fissural explosive eruptions both inside and outside the calderas. The explosive dynamisms were successively or concomitantly strombolian and phreatomagmatic and generated 70 strombolian cones and 3 maars, of which 19 cones and 2 maars are in the interior of the caldera of Eboga. The overall past eruptions have produced a variety of flows and pyroclastic deposits, including volcanic ash, lapilli, and volcanic bombs. The diatremes of Manengouba are carrot-shaped structures filled with volcanic breccia and fragments of country rocks.

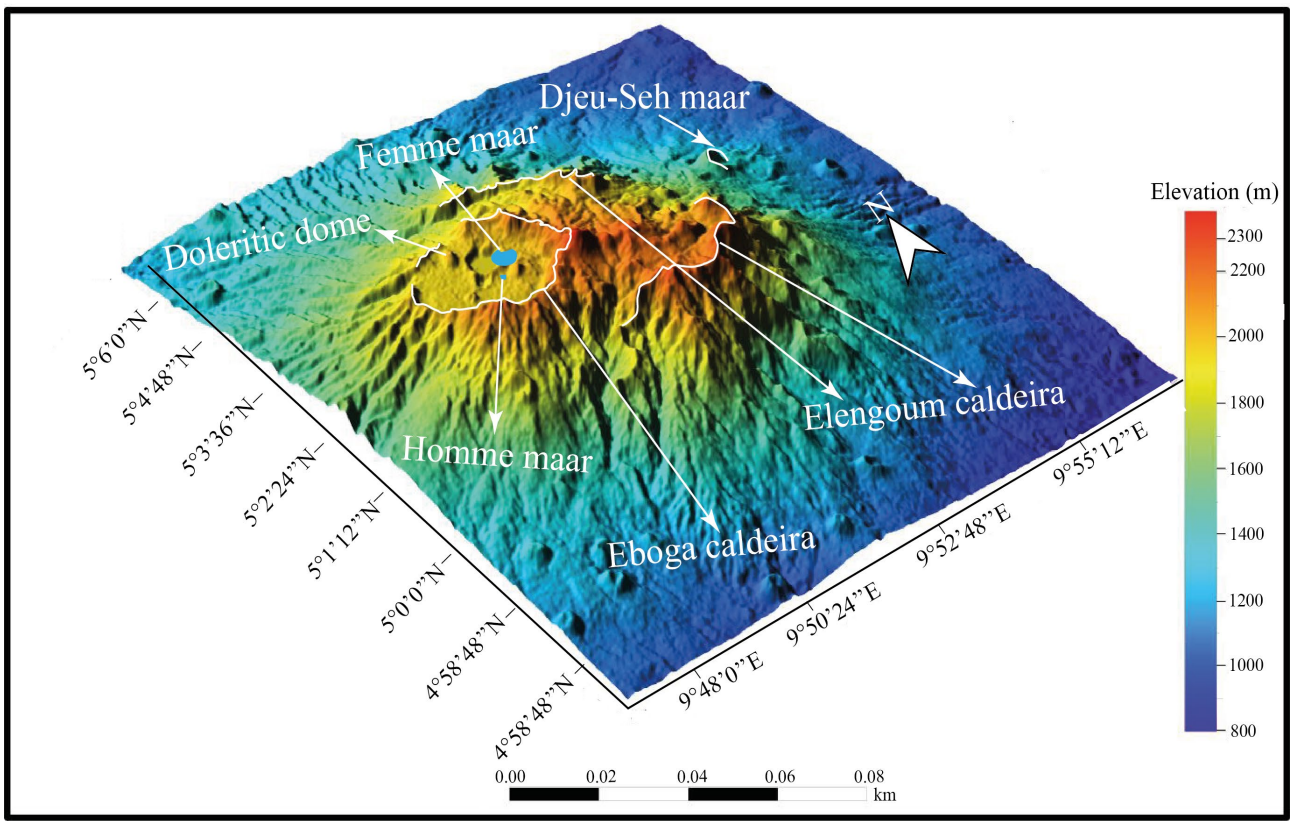

Figure 2. MNT of Mount Manengouba and its surroundings.

The MM volcanics form a complete and an incomplete alkali-sodic volcanic series. The complete series ranges from basanites to quartz-trachytes and is distributed over the whole volcano, while the incomplete one extends from basanites to trachy-andesites and is reduced to late fissure activity confined to the flanks (**Figure 3**). These two series evolved by fractional crystallization and crustal assimilation (Kagou Dongmo et al., 2001; Pouclet et al., 2014). Pouclet et al. (2014) estimated that the magma sources were likely located in the transition zone between garnet- and spinel lherzolites (37 - 39 km for the incomplete series and 42 - 44 km for the other series), and the complete series resulted from a lower melting rate (3% - 6%) of a richer garnet source (3% - 7%). Geochemical analyses of the Manengouba volcanics reveal significant heterogeneity in mantle sources: Sr, Nd, and Pb isotope data portray a three-component mixed mantle source, including a depleted asthenospheric swell component, a lithosphere-contaminated radiogenic component, and a pre-rifting enriched component (Pouclet et al., 2014). Indeed, basalts from this region show enrichments in trace elements such as niobium (Nb) and zirconium (Zr). Isotopic studies also suggest interactions between magma and the continental lithosphere, modifying the chemical composition of the magmas before their eruption (Fitton & Dunlop, 1985).

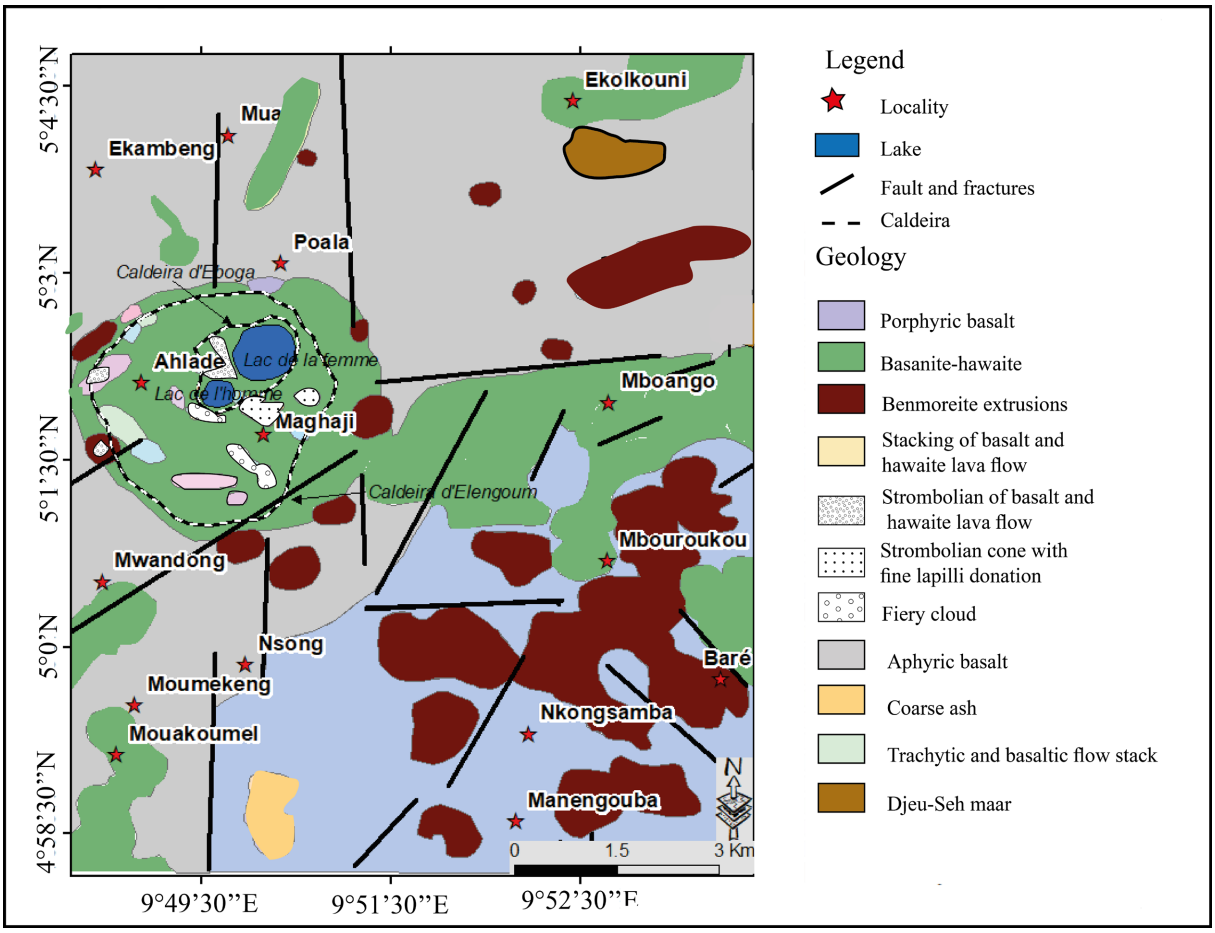

Figure 3. Geological map of pyroclastic deposits of Manengouba maars (from (Pouclet et al., 2014)).

3. Methodology

3.1. Sample Collection

For this study, seven samples of pyroclastic products from the Manengouba maars were selected for petrographic, mineralogical, and geochemical characterization (**Table 1**). Four samples were collected from the Djeu-Seh maar (MDS: P2N3a, P2N3b, P2N4, P2N5), two from the Femme maar (MF: P9, P22), and one from the Homme maar (MH: P23). The samples were collected using a machete and a hand trowel from the internal and external walls of the different maars. Samples taken from the external walls were located approximately 25 meters from each maar. During collection, the top 1.5 cm layer was removed to avoid contamination. Then, 400 grams of pyroclastic material were collected, packed in plastic bags, and transported to the Geosciences Laboratory at the University of Yaoundé I for air drying for three days at 25˚C - 26.5˚C.

For further analysis, 250 grams of each sample were ground using an agate mortar and pestle into a fine powder (<63 μm) for mineralogical and geochemical analyses.

Table 1. Maar sampling points.

Maars	Stratigraphic units	Geographic coordinates	Altitudes
MF	P9	N502'15.7' - E9O49'41.2'	1925 m
	P22	N502'14.2" - E9049'33.,8"	1942 m
MH	P23	N0501'11.4' - E9049'45.4"	1948 m
MDS	P2N3a	N503'08" and E9053'8,7"	1450 m
	P2N3b	N503'8,2" and E9053'7,2"	1462 m
	P2N4	N503'05" and 9053'06"	1470 m
	P2N5	N503'03" - E9053'05"	1597 m

3.2. Petrography and Mineralogy

A Burker diffractometer operating with a Co target (45 mA and 40 kV) with a wavelength of 1.5418 Å was used to determine the mineralogical composition of the pyroclastic samples by X-ray diffraction. The mineralogical composition of the pyroclastics was obtained using the X'Pert High Score Plus software. Thin sections were prepared at the Geological and Mining Research Institute (IRGM) in Yaoundé-Cameroon, and microscopic observations were performed using a binocular microscope (plane polarized light) hosted at the Soil Analysis and Environmental Chemistry Research Unit (SAERU) of the Department of Earth Sciences, University of Dschang (Cameroon). Thin sections were prepared from three pyroclastic samples, including two pumices and one lapilli block.

3.3. Modeling Volcanic Processes

Petrographic and geochemical data were integrated into numerical models to sim-

ulate the volcanic and magmatic processes responsible for the formation of the diatremes and maars of Manengouba. Thermodynamic modeling software was used to simulate the pressure, temperature, and chemical composition conditions during magma crystallization. Dynamic models were developed to understand the interactions between magma and groundwater, as well as the migration of fluids and gases within the diatremes. Differential thermal analysis (DTA for Differential thermal analysis) is used to identify the phase transition temperatures of sample. In this work this method was employed to identify invariant reactions in the Cu-FeO and Cu-Cr-O systems, in addition to defining the eutectic point of the first system. The basis of the measurement is based on the idea that with each phase change of a material, an energy variation in associated with it. This energy conversion is measured in ATD system by heating and cooling an inert substance (reference) and the sample to be analyzed. Thermocouples are used to determine a temperature difference between the two crucibles that occurs during a phase transition. These process, exothermic or endothermic, result in negative or positive peaks respectively in the measured signal. Conversely, if no phase transformation occurs, crucibles heat in the same manner and signal is generated. During the combining DTA with thermogravimétric analysis, it is also possible to determine the mass variation of the sample during the measurement. Specifically, regarding oxides, oxidation or reduction or removal of oxygen, therefore induce measurable changes in mass.

3.4. Geochemistry

Seven samples of juvenile products were selected for bulk rock major, trace, and rare earth element compositions. Major elements were analyzed using an analytical microscope (XGT-2700) at the Institute of Inorganic Chemistry, Christian-Albrechts-Universität zu Kiel, Germany, while trace and rare earth element contents were determined by inductively coupled plasma mass spectrometry (ICP-MS) at ACTIVATION LABORATORIES LTD in Ontario, Canada. The preparation of solutions for each sample followed the method described by Makishima & Nakamura (1997).

First, the geochemical sample powders were dried at 110˚C and then calcined at 1000˚C. The loss on ignition (LOI) at 1000˚C was calculated by the difference in mass between the dried powder and the calcined powder (expressed as a weight percentage of the dry sample). The major elements were analyzed on beads obtained by high-temperature fusion of a mixture of 0.75 g of calcined pyroclastic powder and 4.50 g of lithium tetraborate (Li2B4O7) used as a flux. The major elements and their concentrations in each sample were determined by X-ray fluorescence generated by a rhodium anticathode.

4. Results

4.1. Petrography and Mineralogy

The minerals observed in the different types of rock and their proportion are re-

ported in Table 2.

4.1.1. Petrography

❖ **Pyroclastic Rock**

Whether in flow deposits or pyroclastic fallout, juvenile and lithic fragments exhibit significant petrographic resemblance to the associated basaltic and trachytic flows (i.e., flows from the first effusive phase). The petrography of the pyroclastics from the Manengouba maars was carried out using lithic fragments of pumice and lapilli blocks, juvenile fragments of bombs, basalts, mugearite, and trachyte.

The macroscopic petrography of juvenile fragments of volcanic bombs encountered in the Djeu-Seh and the Homme maars generally reveals fusiform shapes and sometimes ribboned breadcrusts. They are slightly vesicular, basaltic in nature, black in colour, and have an aphyric texture. The bombs are basaltic and black. Microscopic observation of the bombs (Figure 4(a) and Figure 5(a)) reveals that they are made up of phenocrysts and groundmass microcrysts of clinopyroxene, plagioclase, and opaque minerals. Augite phenocrysts represent 3 vol.% of the rock. They are the most abundant minerals in the rock. They appear as subhedral to anhedral phenocrysts and microphenocrysts. Some augite crystals show initial stages of alteration (uralitization) into opaque minerals. These augite crystals range from 0.8 to 4.4 mm along the long axis. Plagioclases represent 15 to 20 vol.% of the rock volume. They appear as subhedral microcrystals with distinct contacts with opaque minerals. Opaque minerals occur either (i) as subhedral microcrystals often included or developed at the expense of augite, or (ii) in contact with plagioclases (Figure 5(a)). Their crystallization seems to have been continuous since the initial stage of magma differentiation until the eruption.

Pumices of the Homme maar are reddish, vesicular, and thus lightweight, decimetre to centimetre across, and weakly weathered. Microscopically, they display vacuolar microlitic porphyritic textures and are composed of pyroxene, olivine, plagioclase, and opaque minerals. Augite and olivine are present both as phenocrysts (1 - 2 and 2 - 5 vol.% respectively), ranging in length from 0.4 to 1.12 mm, and as microcrysts associated with plagioclase (3–8 vol.%) and opaque minerals. Vitreous phases amount to ≈25 vol.%, while vesicles can attain 60 vol.%. The latter have variable sizes and are distributed throughout the rocks (Figure 4(b) and Figure 5(b)).

Lithic fragments of lapilli blocks appear as enclaves within the ashes. Block sizes range from centimetre to millimetre scale. The blocks are trachytic, light-grey in colour, with a mineralogical composition of feldspars and pyroxene. Microscopic observation of these lapilli blocks shows a trachytic texture composed of sanidine, clinopyroxene, and opaque minerals. Sanidine crystals are subhedral to euhedral and represent ≈50 vol.% of the rocks. Some of their phenocrysts are poikilitic (opaque mineral inclusions) or display cracks filled by thin melts containing

opaque mineral microcrystals (Figure 4(c) and Figure 5(c)). Phenocryst sizes range between 0.92 and 2.32 mm along the long axis. Augite represents 3 vol.% of the rock volume. They occur as poikilitic phenocrysts (0.56 - 1.12 mm in length) and microcrystals. From the above, the crystallization order can be drawn as follows: opaque minerals-clinopyroxene-sanidine.

❖ **Lava flows**

Homme Maar

The effusive phase corresponds to basaltic lava with an aphyric microlithic texture, slightly vesicular. Some of its vesicles are filled by sub-solidus crystals. Microscopic observation reveals the following minerals: olivine, clinopyroxene, plagioclases, and opaque minerals (Figure 5(d)). Olivine and augite appear as microphenocrysts embedded in a matrix consisting of plagioclase and olivine microlites. Olivine crystals vary widely in size (0.34 to 1.92 mm for longitudinal sections) and represent ≈20 vol.% of the rocks. They exhibit numerous fractures and are not in contact with other minerals. Augite (5 vol.%) occurs as subhedral to euhedral microphenocrysts. Crystal sizes range from 0.17 to 1.63 mm. Some augite and ilmenite crystals are in contact, with straight borders. Labrador-oligoclase occurs as microlites dispersed in the rock without contact with other crystals. The mesostasis is generally holocrystalline and microlitic, containing dominant plagioclase microlites. Microscopic observation shows the crystallization order as follows: olivine, augite, ilmenite, and finally plagioclase.

Femme Maar

The first effusive phase is represented by greyish trachytic flows. In thin sections, they exhibit the characteristic trachytic texture and contain sanidine, augite, plagioclase, and opaque minerals (Figure 4(d) and Figure 5(e)). Augite phenocrysts are embedded in a matrix poor in volcanic glass, sanidine microlites, and opaque minerals. Clinopyroxene crystals (15 vol.%) are subhedral to anhedral and display a bimodal distribution, with subhedral phenocrysts averaging between 0.8 and 1.12 mm along the long axis. They are rarely twinned and are sometimes associated with opaque minerals. Microphenocrysts (0.32–0.4 mm) are anhedral and associated with sanidine and ilmenite-titanomagnetite crystals. Sanidine crystals (35 vol.%) also exhibit a bimodal distribution, with euhedral to subhedral phenocrysts up to 1.8 mm along the long axis and more abundant microcrystals averaging 0.01 mm. They show Carlsbad twins and are associated with augite. Opaque minerals are subhedral to euhedral, occurring as inclusions within augite.

The second effusive phase is represented by an alkaline basaltic flow with a microlitic porphyritic texture, composed of clinopyroxene and plagioclase phenocrysts (Figure 4(e), Figure 4(f) and Figure 5(f)). Two bands with greenish trends, consisting of fine olivine grains, are also observed. The basalts, exposed on the internal walls of the Femme maar, are deep grey. Augite crystals (20 vol.%) are subhedral to euhedral with a bimodal distribution. Subhedral phenocrysts have average sizes between 2.28 and 3.05 mm along the long axis and are often poikilitic, associated with

opaque mineral crystals. Microphenocrysts are anhedral and associated with plagioclase and opaque mineral crystals, with sizes ranging from 0.13 to 0.26 mm along the long axis, also showing initial stages of alteration by opaque minerals. Labradorite (50 vol.%) are the most abundant crystals in the rock, appearing as euhedral to subhedral phenocrysts and microphenocrysts. They have an elongated rod shape with sizes up to 4 mm along the long axis.

Djeu-Seh Maar

Trachytes represent pre-maar volcanics in the Djeu-Seh area, thus constituting the walls of the Djeu-Seh maar. They are light grey in colour and exhibit a fluidal microlitic porphyritic texture containing mainly sanidine, clinopyroxene, plagioclase, and opaque minerals. Sanidine and augite crystals occur as phenocrysts and microphenocrysts embedded in a fine matrix containing all the rock mineral phases and a small amount of volcanic glass. Sanidine (35 vol.%) appears as subhedral to anhedral phenocrysts and microlites with sizes of 2.92 – 4 mm and approximately 0.12 mm, respectively. Augite (10 vol.%) occurs as subhedral phenocrysts with crystal sizes of about 2.8 mm along the long axis and often encloses opaque mineral microcrysts. Titanomagnetite crystals are sub-rounded, with sizes ranging from 0.02 to 0.12 mm (**Figure 4(g)** and **Figure 5(j)**).

The foot of the north-eastern outer flank exhibits layered basaltic deposits (**Figure 4(h)-(j)** and **Figure 5(h)-(k)**). The bottom layers are thick and made up of coarse and often agglomerated blocks, while the upper layers are thin and their particles loose. Under thin section (sample MGZ14), these rocks are subaphyric microlithic and composed of olivine, clinopyroxene, plagioclase, and opaque minerals. Olivine and augite crystals appear as phenocrysts in a matrix of volcanic glass and microlites of plagioclase and ilmenite. Plagioclases (35 vol.%) appear as subhedral microlites with distinct contacts with opaque minerals. Augite crystals (20 vol.%) are subhedral to anhedral, with some poikilitic crystals showing initial stages of uralitization. Crystal sizes range from 0.8 to 4.4 mm along the long axis. Olivine (5 vol.% and 0.6 to 1.86 mm) occurs as anhedral phenocrysts and microphenocrysts; phenocrysts are highly fractured and mostly deeply iddingsitized. Ilmenite minerals appear as anhedral microcrystals and microlites, often included in clinopyroxenes and plagioclases.

Mugearite (MGZ17) outcrops as a prismatic flow with a few vacuoles. It is deep-grey in color, microlitic porphyritic in texture, and made up of plagioclase, augite, basaltic hornblende, and titanomagnetite. Plagioclase (3 to 20 vol.%), augite (10 vol.%), and kaersutite (3 to 5 vol.%) occur as euhedral to subhedral phenocrysts and microcrysts, while opaque minerals occur merely as sub-rounded microcrysts. Plagioclase elongated crystals range in size between 0.08 and 1.28 mm. Basaltic hornblende crystals are often poikilitic and exhibit a thick oxidized border: the oxidation sometimes invades almost the entire crystal, leaving only a brown remnant core. Titanomagnetite is either primary or secondary, the latter resulting from the alteration of brown hornblende (**Figure 4(k)** and **Figure 5(l)**).

Table 2. Summary table of the different samples and their mineralogical composition.

	Male maar				Female maar				Djeu-Seh Maar			
Samples	Texture	Cristal sizes	Phenocrystals	Mesostasis	Texture	Phenocrystals	Cristal sizes	Mesostasis	Texture	Phenocrystals	Cristal sizes	Mesostasis
Basalts	Aphyric microlitic	0.34 - 1.92 mm	-Olivine (35%) -Clinopyroxene (20%) -Plagioclase (10%)	Plagioclase (5%) Oxides (20%) Volcanic (10%) glass	Porphyric microlitic	Olivine (20 - 25%) Clinopyroxene (10 - 15%)	Ol (1.2 - 4 mm) Cpx (0.88 mm)	Oxide (10 - 15%) Volcanic glass (30 - 45%)	Aphyric microlitic	Olivine (35%) -Clinopyroxene (20% - 25%) -Plagioclase (15% - 20%)	0.19 - 1.86 mm 0.8 - 4.4 mm 0.12 - 0.18 mm	Oxides (5% - 10%) Volcanic glass (15%)
Mugearite	-	-	-	- -	-	-	-	-	Aphyric microlitic	Hornblende (30% - 35%) Clinopyroxene (15% - 20%)	1.08 - 1.30 mm 0.3mm	Plagioclase (30% - 25%) Oxides (5% - 10% Volcanic glass (2 - 8%)
Trachyte	-	-	-	- -	Trachytic texture	Clinopyroxene (20 - 25%) Sanidine (30 - 35%)	Cpx (0.8 - 1.8 mm) Sa (1.12 mm)	Oxides (15 - 25%) Sanidine (5 - 10%)	Trachytic texture	Clinopyroxene (20% - 25%) plagioclase (35% - 40%)	2.03 - 3.05 mm 4 mm	Oxides (2% - 10%) Plagioclase (30% - 35%)
Pumice	Vesicular	Clinopyroxene (10% - 15%) Plagioclase (50%)	0.56 - 1.12 mm 0.92 - 2.32 mm	Oxides (10% - 15%) Plagioclase (20%)	-	-	-	-	-	-	-	-
Juvenile fragments of trachytic block	Trachytic texture	Clinopyroxene (10% - 15%) Plagioclase (50%)	0.56 - 1.12 mm 0.92 - 2.32 mm	Oxides (10% - 15%)/ 0.01 - 0.05 mm Plagioclase (20%)								
Volcanic bombs	Vesicular	Olivine (5% - 10%) Clinopyroxene (10% - 15%) Plagioclase (5%)	0.2 - 0.23 mm 0.56 - 1.12 mm 0.92 - 2.32 mm	Oxides (10% - 15%) Plagioclase (20%) Volcanic glass (50%)					Vesicular	Olivine (10%) Clinopyroxene (10% - 15%) Plagioclase (3%)	0.2 - 0.23 mm 0.56 - 1.12 mm 0.92 - 2.32 mm	Oxides (10 - 15%) Plagioclase (20%) Volcanic glass (52%)

Figure 4. Photograph of rock samples from the Manengouba maars.

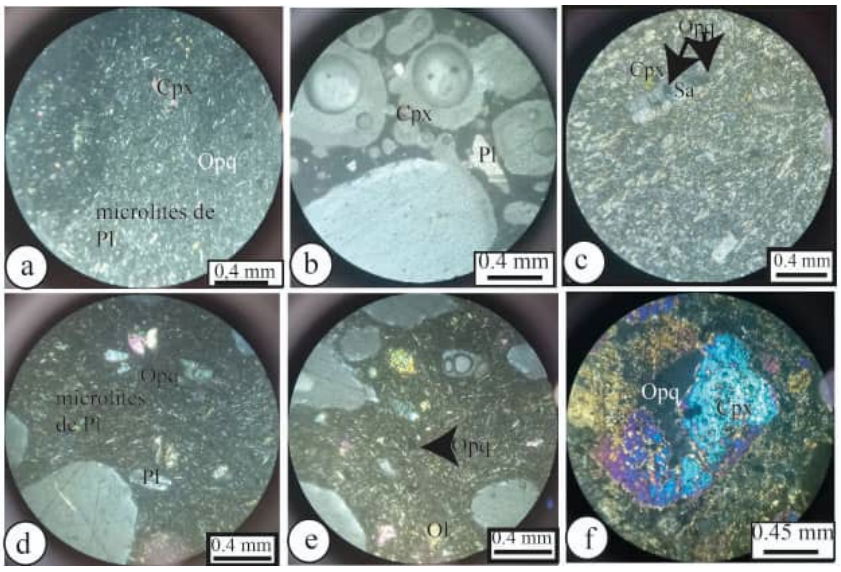

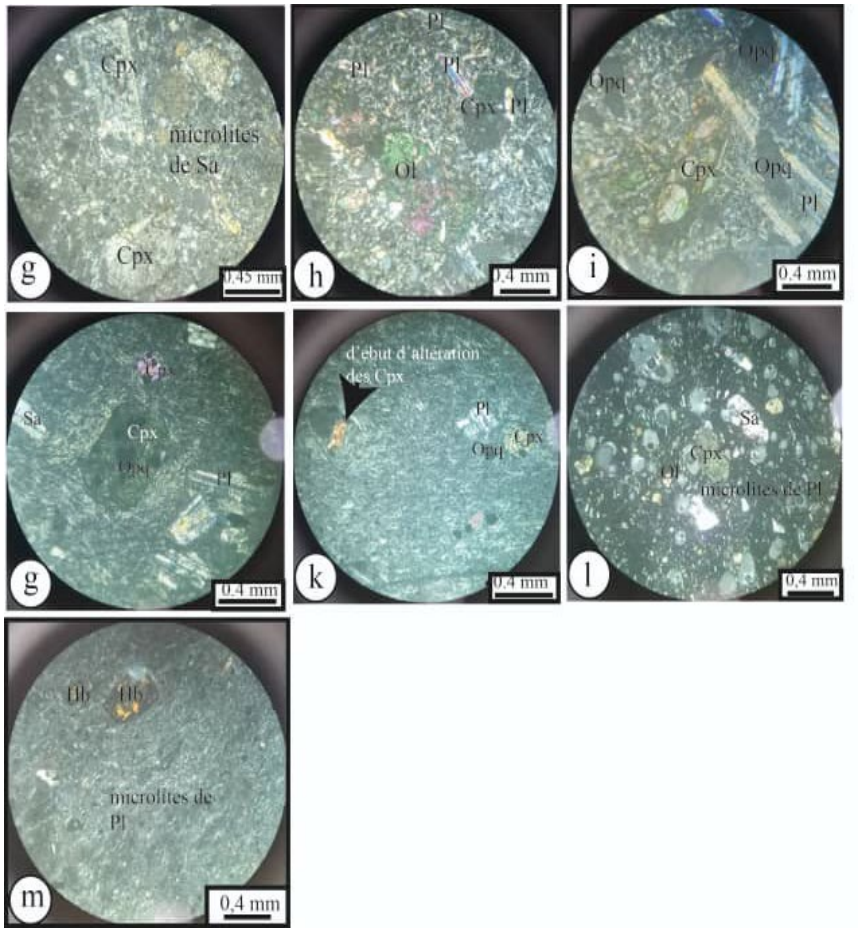

Figure 5. Photomicrograph of thin sections of rock from the Manengouba maars.

4.1.2. Mineralogy by X-Ray Diffraction (XRD)

XRD analyses revealed varied mineralogical compositions in the pyroclastic deposits of the Manengouba Maars. Diffractograms (Figure 6) reveal the presence, in addition to the primary minerals described in the petrography section, of weathering minerals, often in significant quantities. XRD analyses revealed varied mineralogical compositions in the pyroclastic deposits of the Manengouba maars. Djeu-Seh Maar: The diffractograms of the samples show high proportions of smectite (25.99% to 76.05%), moderate amounts of olivine (4.79% to 14.83%), potassium feldspars (9.67% to 13.26%), and plagioclases (5.93% to 19.72%). Pyroxenes are present in low quantities (1.23% to 6.54%) along with hematite. Oxides such as maghemite-magnetite and hydromagnesite are present in almost all samples, with proportions ranging from 2.01% to 10.83%. Male Maar: The results show a high abundance of smectite (71.28% to 76.05%), moderate quantities of olivine, pyroxene, and plagioclase, as well as traces of serpentine, potassium feldspars, and amphibole. Clay minerals such as kaolinite and smectite are also present in significant amounts (50.62% to 76.05%). Female Maar: Smectite is abundant (25.99%), with moderate amounts of olivine (9.63%), plagioclase (3.70%), and oxides such as maghemite-magnetite.

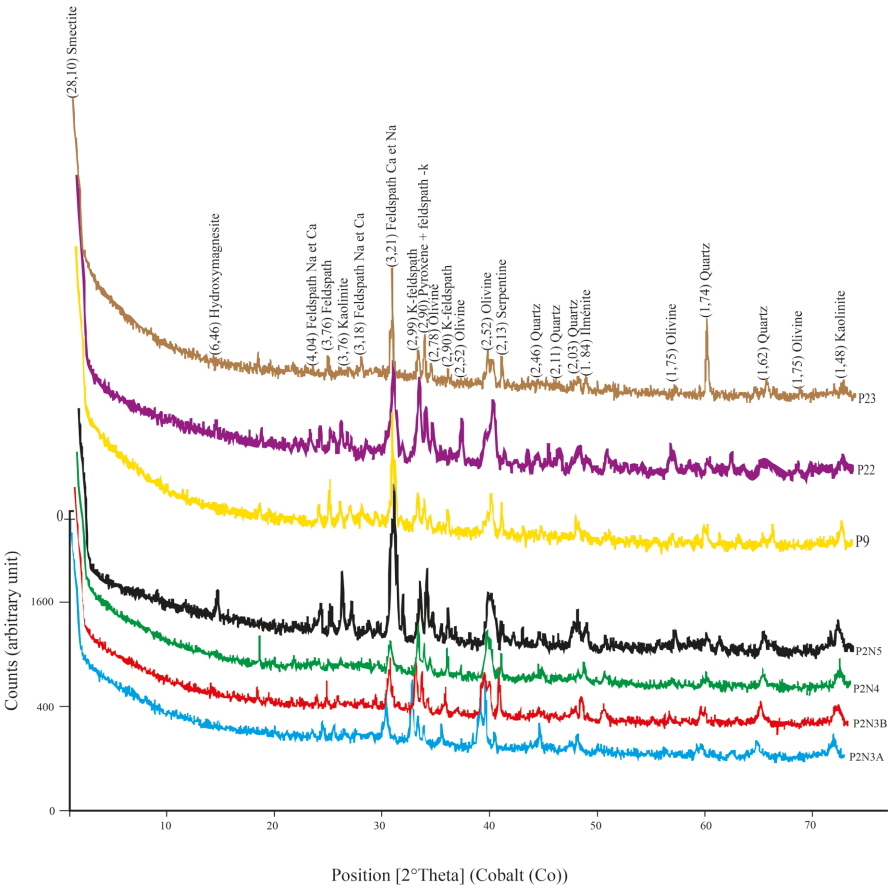

Figure 6. Diffractograms of the pyroclastic deposits of the Manengouba Maars.

Table 3 shows that the primary minerals are, in decreasing order: plagioclase (5.93 - 19.72 vol.%), olivine (4.79 - 14.83 vol.%), alkali-feldspars (9.67 - 13.26 vol.%), magnetite (2.01 - 10.83 vol.%), and pyroxenes (1.23 - 6.54 vol.%). In a similar order, the weathering minerals are as follows: smectites (25.99 - 76.05 vol.%), kaolinite (5 - 10 vol.%), serpentine, and hydromagnesite (in traces). The distribution of pelites is not balanced between the different maars: the pyroclastites of the two maars contain more smectites, but less kaolinite and serpentine than the Djeu-Seh Maar.

Table 3. Mineral composition of altered pyroclastites from the Manengouba maars.

	Pyroclastic of Djeu-Seh maar				Pyroclastic of Femme maar		Pyroclastic of Homme maar
Samples	Medium lapilli	Fine lapilli	Medium lapilli	Fine lapilli	Medium lapilli	Medium lapilli	Medium ash
Ref: code	P2N3a	P2N3b	P2N4	P2N5	P9	P22	P23
Quartz	+++	-	-	+	-	+	-
Olivine	+	++	++	++	-	+	-
pyroxene	-	+	+	++	-	++	+
Kaolinite	++	++	++	+	+	-	-

Continued

K-feldspars	++	++	++	++	+	+	-
Plagioclase	-	++	-	+++	-	+	-
Amphibole	-	-	-	+	-	+	-
Serpentinite	-	-	-	+	+	+	+
Ilmenite	++	-	-	+	-	-	-
Smectite	+++	+++	+++	+++	++++	++++	+++
Hydromagnesite	-	-	-	+	-	-	-
Magnetite-maghemite	-	++	++	++	+	+	++

+++++ = Very abundant; ++++ = abundant; +++ = moderaly represented; ++ = Poorly represented; + = trace; - = not identified.

4.2. Geochemistry

The geochemical analyses of the different samples are reported in **Table 4**.

4.2.1. Alterability

Pyroclastic rocks in general, and fine clasts in particular, are readily weathered, modifying to some extent their composition. We evaluate the impact of weathering on the pyroclasts of the Mount Manengouba maars, using the alteration box (**Figure 7** after (Large et al., 2001)), which combines the Chlorite-Carbonate-Pyrite

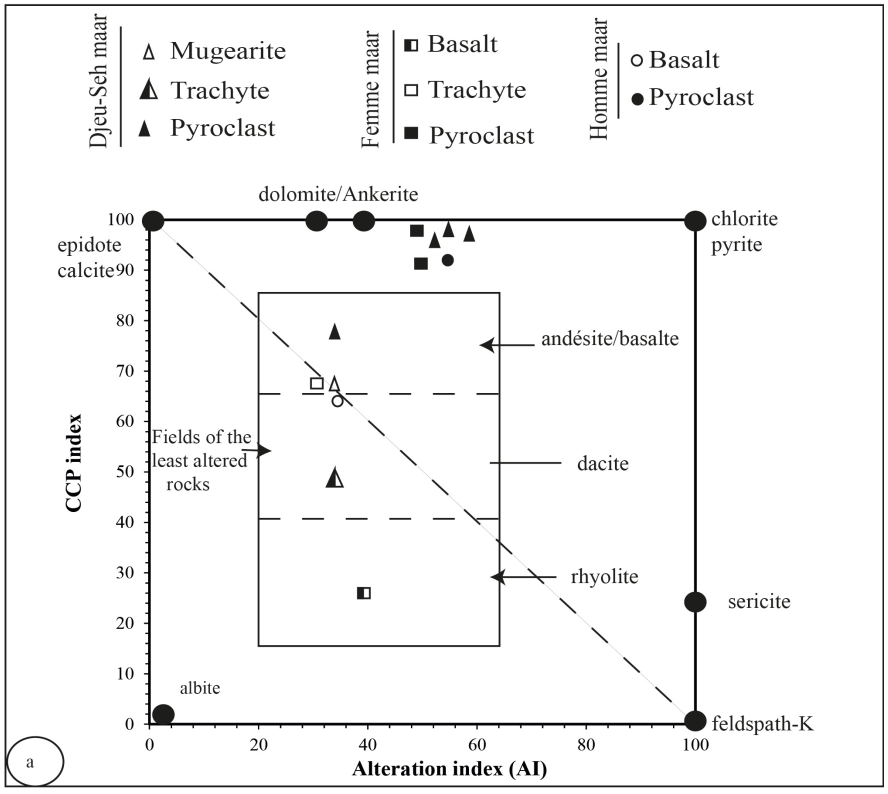

Figure 7. Alteration diagram of the pyroclastic deposits of the Mount Manengouba maars. The alteration box is from Large et al. (2001); the Chlorite-Carbonate-Pyrite Index is from Lentz (1996, 1999) and the Alteration Index is from Ishikawa (1976).

Index diagram (CCPI) (Lentz 1996, 1999) and the Ishikawa Alteration Index (IA, Ishikawa et al., 1976). The pyroclastic deposits of the Djeu-Seh and the Femme Maars exhibit high weathering indexes, with respectively: AI between 52.84 - 56.41 and 36.10 - 53.93, and CCPI from 95.83 - 96.45 and 76.44 - 98.11. On the contrary, only a single sample from the Homme Maar shows a high alteration rate (P9: IA = 51.09 and CCPI = 96.45). The degree of weathering correlates negatively with the contents of the major elements SiO_2, Na_2O, and K_2O. This correlates with the extremely low proportions of certain major elements. However, the increase in alteration indices in the pyroclastic rocks found in the various maars suggests that SiO_2, Na_2O, and K_2O have been leached. Additionally, these high AI values are consistent with the findings of Large (2001), indicating that rocks with an AI between 50 and 100 have undergone hydrothermal alteration.

4.2.2. Classification and Nomenclature

As recommended by the IUGS, volcanic rocks should be named using the total alkali vs. silica diagram of Le Bas et al. (1986). **Figure 8** shows, however, that most of the studied rocks display AI above 50, indicating that they suffered a consistent degree of hydrothermal alteration (Large et al., 2001). In such cases, alkalis and silica are among the most leached-out elements. Immobile elements, since they are less sensitive to hydrothermal alteration, therefore become the viable alternative for the nomenclature. In this light, we use the Zr/Ti vs. Nb/Y diagram after Floyd and Winchester (1977) for the nomenclature of the volcanics of the Mount Manengouba Maars (**Figure 8**). Pyroclasts from the three maars plot in the field of alkaline basalts.

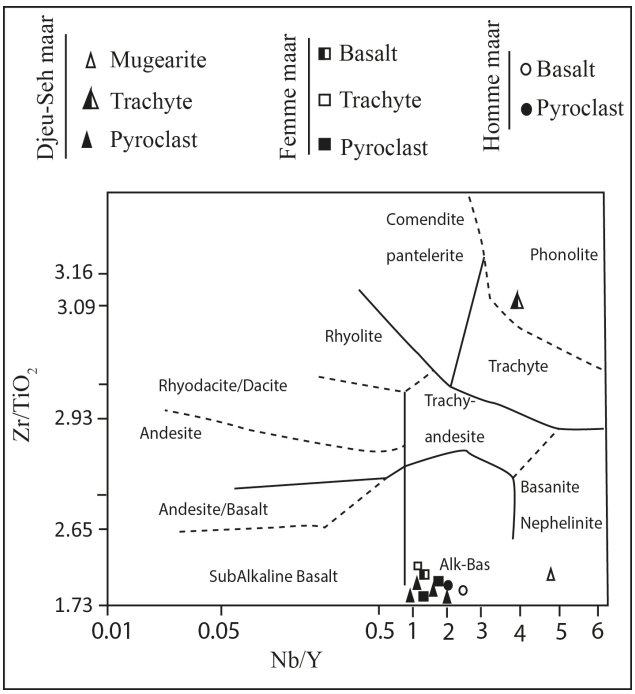

Figure 8. Zr/Ti vs. Nb/Y classification diagram of the pyroclastites of Manengouba maars. Field boundaries as defined by Floyd & Winchester (1977) and modified by Pearce (1996).

4.2.3. Major Element Compositions

The magnesium number (Mg# = Mg/(Mg + Fe2+)), calculated on the basis of Fe_2O_3/FeO of 0.15 for pyroclastites and the basalt MGZ11 and 0.65 for the remaining rocks, gives values in the range of 0.2 - 0.38 for intermediate and evolved rocks and 0.35 - 0.54 for pyroclastites. Pyroclastites from the Homme Maar are the most evolved (Mg# = 0.31 - 0.35), while a pyroclastite from Djeu-Seh is the most basic (Mg# = 0.54) of our spatters. MgO varies between 0.54 and 10.49 wt.% over the data set and between 5.72 - 10.49 wt.% in pyroclastites. Apart from two Djeu-Seh samples with the extreme values, most of these pyroclastites have contents clustering around 6 wt.%. FeOt also spans a wide range of contents, i.e., 4.94 - 24.8 wt.%, with a gap between pyroclastites and the rest of the set. Concerning pyroclastites, the FeOt contents range between 15.22 - 24.8 wt.%, with the highest values recorded at Djeu-Seh and the Homme Maar. Al_2O_3 exhibits a closer range of values with respect to MgO and FeOt, within the bracket of 11.26 - 17.54 wt.%. Pyroclastite contents vary from 12.24 - 16.42 wt.%, the bracketing values being recorded at Djeu-Seh. TiO_2 compositions vary from 0.57 - 4.69 wt.%, with pyroclastites displaying a short range (3.11 - 4.69 wt.%). CaO compositions vary widely over our set of data (2.03 - 10.04 wt.%) as well as in pyroclastites (4.71 - 10.04 wt.%), though the two maars or lakes display comparable values (4.71 - 5.11 wt.%).

Binaries of selected major elements vs. MgO (**Figure 9**) portray a gradual and regular decrease in Al_2O_3 from the pyroclastites of the Djeu-Seh maar to the Homme maar, and in TiO_2, FeOt, and P_2O_5 from the pyroclastics of the Djeu-Seh maar to the Femme maar. Conversely, there is an increase in K_2O, Na_2O, and CaO from the pyroclastites of the Homme maar to the Djeu-Seh maar.

4.2.4. Trace Element Compositions

Trace element compositions are very dispersed. Cr contents vary widely over the entire data set (5 - 138 ppm), but moderately in pyroclastic rocks (66 - 138 ppm) and are close in the two maars patterns (91 - 115 ppm). The other transition metals, Co and Ni, behave similarly: 0.5 - 52.6 and 1.7 - 185 ppm, respectively, in the whole set, 34.5 - 52.6 and 80.1 - 157 ppm in pyroclastites, and 42.6 - 45.2 ppm and 112 - 155 ppm in the two maars scoriae. Cu shows a narrow range of compositions in the pyroclastites (48.5 - 62.5 ppm). High field strength elements (HFSE) have comparable values in the two maars fallouts: Zr (228 - 239 ppm), Hf (3.4 - 3.6 ppm), and Nb (57.5 - 60.2 ppm). However, these variations mirror those of the transition metals, both in the global data set and in the pyroclastic rocks as a whole, with respectively: Zr (226 - 791 and 228 - 425 ppm), Hf (3.4 - 17.9 ppm and 3.4 - 7.2 ppm), and Nb (56.3 - 123 ppm and 56.6 - 73.6 ppm). Large ion lithophile element (LILE) contents in the two maars patterns show no particular trend compared to transition metals and HFSE, although they also vary widely in the data set as well as in the three maars pyroclastites: Ba (144 - 874 and 144 - 556 ppm), Rb (1.5 - 93.4 and 1.5 - 41 ppm), and Sr (81.7 - 872 ppm and 81.7 - 757 ppm).

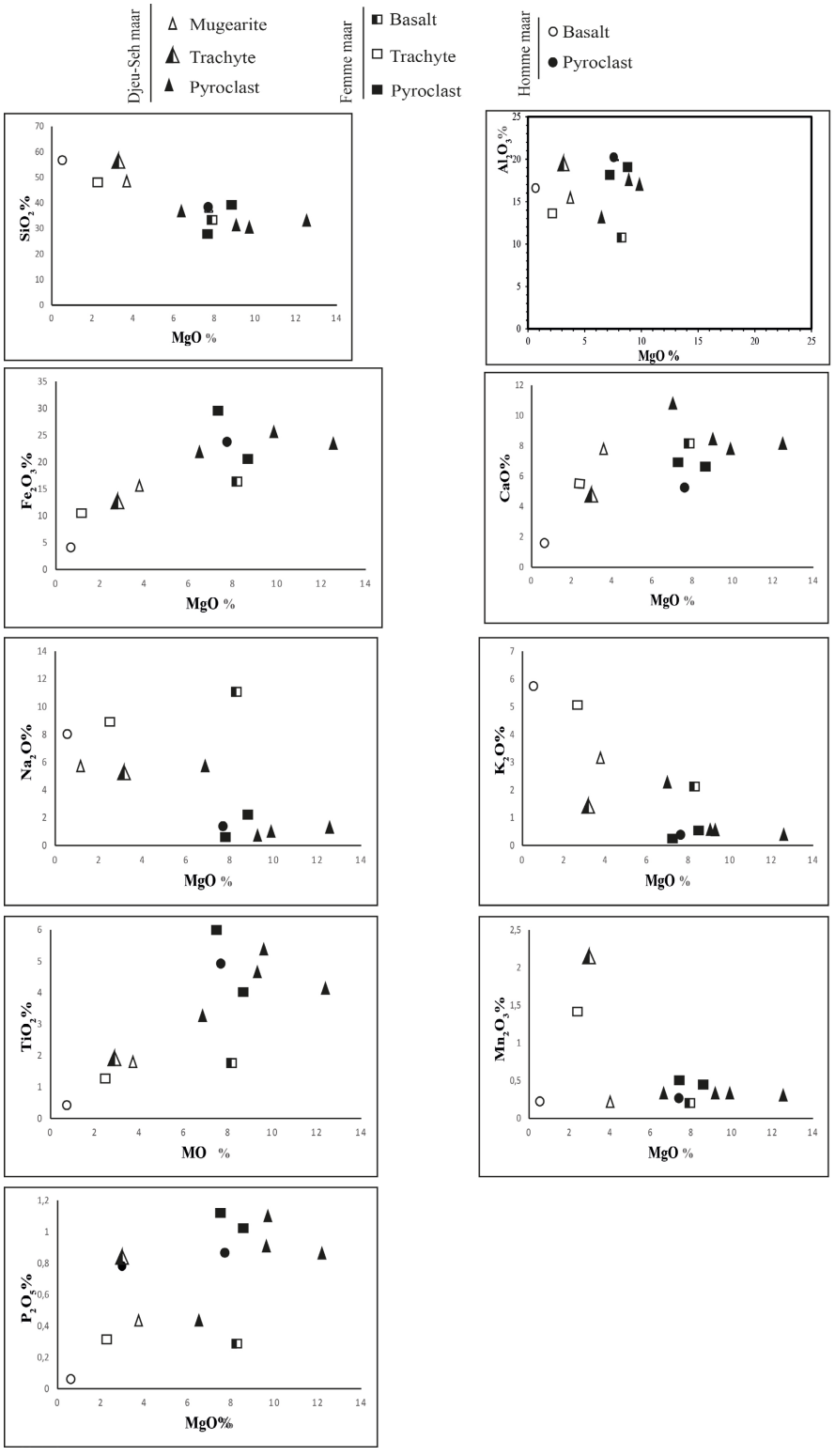

Figure 9. Binary Harker diagram of major elements versus MgO

Binaries of Zr vs. selected trace elements (Figure 10) portray grossly the behaviors described above, with the exception of U and Th whose representative points of pyroclastites define a pattern reminiscent of an open bowl.

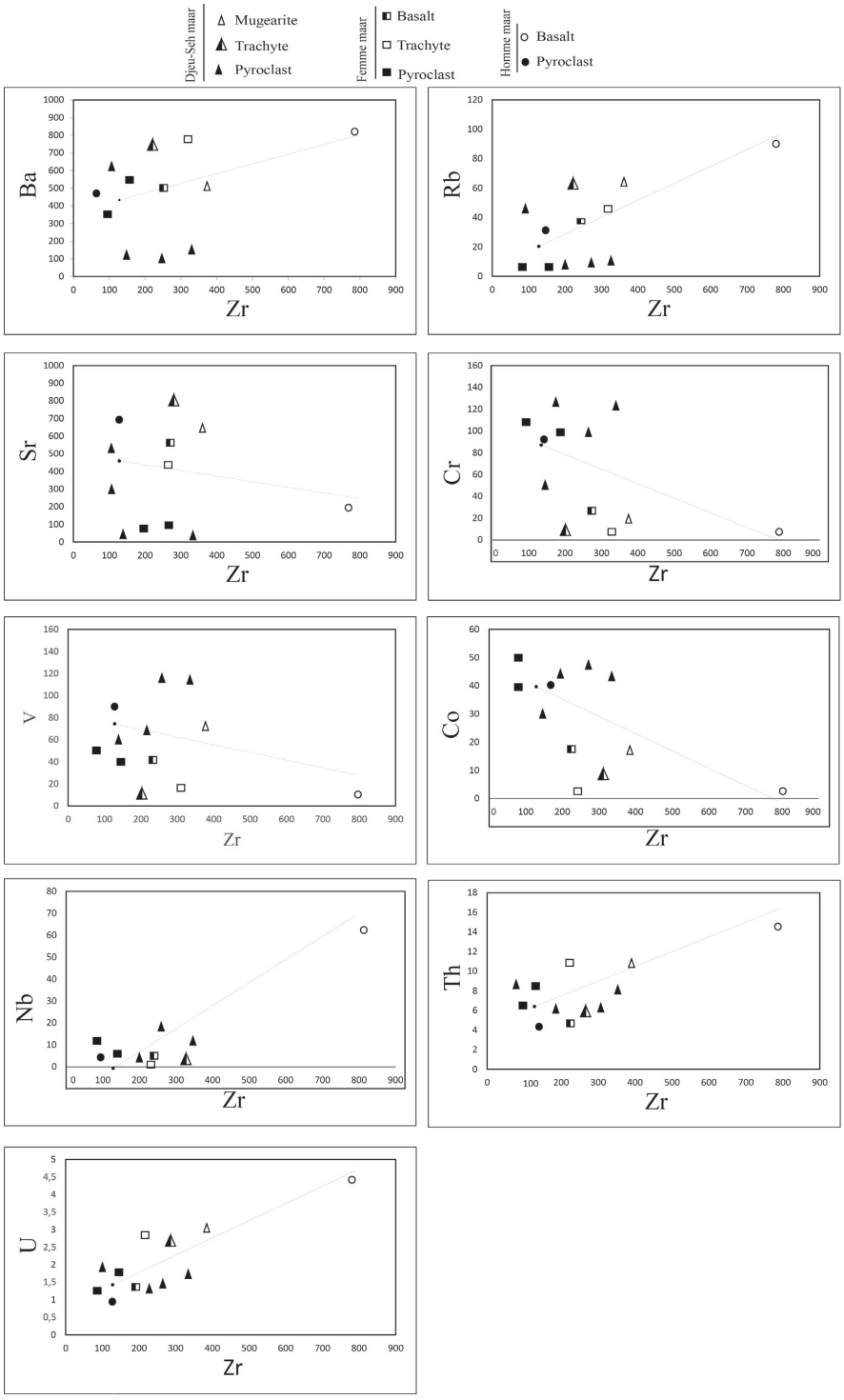

Figure 10. Variation diagrams of selected trace elements versus Zr.

4.2.5. Rare Earth Element Compositions

Rare Earth Elements (REE) normalized diagrams of pyroclasts from the Manengouba maars reveal that they are enriched with respect to chondrites (Figure 11(a)) and to the Primordial Mantle (Fig. not shown). The enrichment relative to chondrites ranges between 11.8 for Lu and 321 for La. Indeed, Light Rare Earth

Elements (LREE) are strongly enriched with respect to Heavy Rare Earth Elements (HREE); La/Yb ratios range from 17.7 to 28.86. All the curves are sub-parallel, with a weak Eu negative anomaly for a Njeu-Seh Mugearite.

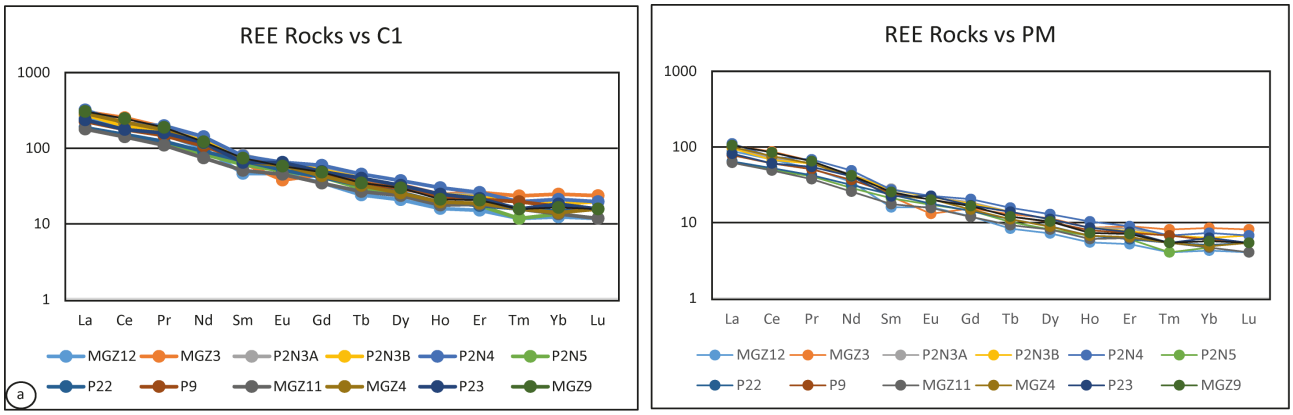

Figure 11. Normalization spectra of the rare Earth elements of the pyroclastites of the Manengouba maars in relation to the primitive mantle and the chondrites according to McDonough & Sun, 1995.

Chondrite Multi-Elements (ME) normalized diagram (**Figure 12**) and PM ME normalized diagram (not shown) show overall similar patterns, especially with respect to the severe negative anomalies in Rb, Pb, and P. Differences appear, however, in the behavior of Hf and Ti: pyroclasts from Njeu-Seh show slight negative anomalies in Hf, but not in Ti, whereas some of the two maars pyroclasts display slight negative anomalies in Ti (**Figure 12**).

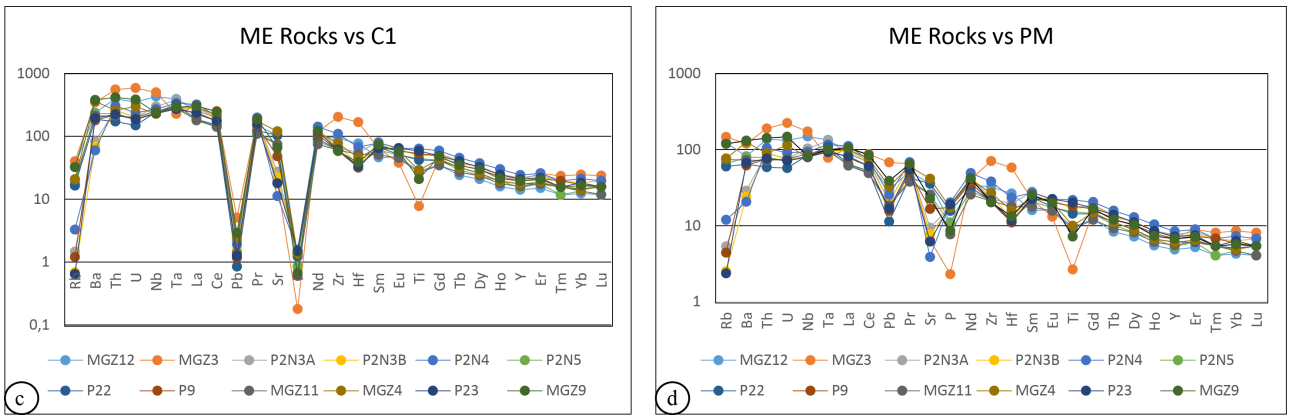

Figure 12. Normalization spectra of the trace elements of the pyroclastites of the Manengouba maars in relation to the primitive mantle and the chondrites according to McDonough & Sun (1995).

Table 4. Synthesis of geochemical characteristics of ptroclastic rocks of Manengouba maars (MH, MF and MDS).

	Djeu-Seh Maar						Female maar				Male Maar	
Rocks	Mugearite	Trachyte	Pyrocl				Pyrocl		Basalt		Trachyte	Pyrocl	Basalt
Sample codes	MGZ12	MGZ3	P2N3A	P2N3B	P2N4	P2N5	P22	P9	MGZ11	MGZ4	P23	MGZ9	
Major elements													
SiO_2	46.485	59.473	28.694	23.027	31.142	35.19	25.211	30.246	35.637	50.447	21.933	48.787	

Continued

TiO2	2.084	0.573	3.692	3.629	4.693	3.301	3.107	3.935	1.96	2.15	4.351	1.547
Al_2O_3	15.482	17.544	13.795	12.24	16.783	12.617	13.887	16.422	11.277	17.173	14.211	14.317
FeOt	13.464	4.939	19.465	17.817	24.8	20.333	15.232	18.813	17.211	10.823	23.223	11.122
MnO	0.248	0.163	0.316	0.254	0.35	0.351	0.223	0.268	0.312	0.277	0.335	0.28
MgO	3.681	0.539	10.494	6.838	9.074	6.573	6.017	6.357	7.786	2.825	5.722	2.302
CaO	7.232	2.031	7.211	5.579	7.833	10.037	5.107	4.709	8.117	4.01	5.06	5.634
Na_2O	6.081	8.412	1.073	0.703	0.881	5.873	1.24	0.866	11.295	5.234	0.506	9.004
K_2O	3.094	5.908	0.228	0.202	0.365	2.419	0.26	0.171	2.213	1.54	0.051	5.078
P2O5	0.481	0.1	0.777	0.742	0.879	0.465	0.683	0.754	0.335	0.746	0.831	0.373
Cr2O3	0.032	0.003	0.046	0.039	0.058	0.029	0.033	0.042	0.027	0.004	0.049	0.003
Total	98.364	99.685	85.791	71.07	96.858	97.188	71	82.583	96.17	95.229	76.272	98.447
MgO+FeO3	17.145	5.478	29.959	24.655	33.874	26.906	21.249	25.17	24.997	13.648	28.945	13.424
Mg#	21.47	9.84	35.03	27.73	26.79	24.43	28.32	25.26	31.15	20.7	19.77	17.15
Na_2O+K_2O	9.175	14.32	1.301	0.905	1.246	8.292	1.5	1.037	13.508	6.774	0.557	14.082
Trace Elements												
Ba	571	836	202	168	144	556	451	433	511	874	467	914
Co	19.9	0.5	52.6	47.8	49	34.5	42.6	44.4	18.8	12.9	45.2	5.8
Cr	27	6	114	128	138	66	91	115	26	9	98	5
Cs	1.19	0.5	0.07	<0.05	0.18	0.39	0.41	<0.05	0.71	0.53	0.11	0.47
Cu	16.8	1.7	54.3	55.4	56.8	48.2	55.7	62.4	56.2	9.2	62.5	4
Ga	17.4	27.6	24.2	23.3	26.4	21	17.5	20.2	21.6	19.1	20.3	19.6
Li	12.7	25	4.8	3.2	6.4	11.7	7.3	4.2	5.6	11	6.4	14.9
Mo	1.73	1.06	0.31	<0.05	0.15	0.23	0.61	0.09	0.47	0.1	<0.05	0.32
Ni	38.9	<0.5	185	151	157	80.1	119	155	35	5.9	112	1.7
Rb	78.4	93.4	3.4	1.6	7.6	41.1	38.1	2.8	47	48.6	1.5	75.3
Sc	9	3	28	24	24	19	24	26	12	7	27	7
Se	0.1	<0.1	0.4	<0.1	<0.1	0.4	<0.1	<0.1	0.3	<0.1	0.2	<0.1
Sn	<1	6	<1	<1	<1	<1	<1	<1	<1	<1	<1	<1
Sr	745	137	199	163	81.7	542	757	350	540	872	130	478
V	89	1	135	72	135	60	83	54	56	30	48	15
W	0.5	0.3	<0.1	<0.1	<0.1	<0.1	<0.1	<0.1	<0.1	<0.1	<0.1	<0.1
Y	22.1	32.1	34.6	33.1	38.2	24.2	27.7	30.6	25.2	27.6	32.7	30.7
Zn	91	122	101	89.1	111	132	102	110	97.8	121	114	110
Pb	5.5	12.6	3.8	3.8	4.7	3.3	2.1	2.9	3.4	6.1	3.1	7.2
Th	11.6	16.1	7.6	7.5	8.9	6.7	5	6.4	6.1	7.6	6.5	12.1
U	2.8	4.7	1.6	1.6	1.9	1.5	1.2	1.5	1.6	2.4	1.5	3.1

Continued

HFSE												
Zr	361	791	252	283	425	235	236	228	235	301	239	226
Hf	8.2	17.9	6	3.7	7.2	3.7	3.4	3.4	5.5	4.9	3.6	4.1
Nb	106.1	123.1	73.6	56.9	67	56.6	60.2	57.9	62.4	56.3	57.5	58.8
Ta	5.5	3.2	5.33	3.98	4.77	3.86	4.46	4.09	4.1	3.96	3.8	4.1
REE												
La	60.6	72	68.8	65.9	76.2	43.9	44.3	53.6	42.4	68.6	56.2	72.4
Ce	121	155	126	120	131	87.7	93	108	86.6	135	108	151
Pr	14.3	18	17	16.6	18.9	11.3	11.7	14	10.4	16.7	15.1	17.9
Nd	46.8	55.5	58.7	58.2	66.4	39	42.7	49.7	34.8	54.7	55.3	56.9
Sm	7.1	9.8	12.4	12.1	12.1	9.3	10.4	10.9	7.8	10.2	9.9	11.3
Eu	2.7	2.2	3.65	3.64	3.78	2.9	2.99	3.38	2.62	3.43	3.76	3.37
Gd	7.2	9.2	11.1	10.6	12.2	8.6	8.5	9.9	7.1	8.9	10.1	9.9
Tb	0.9	1.4	1.5	1.5	1.7	1.1	1.2	1.3	1	1.2	1.5	1.3
Dy	5.3	8.4	8.1	8.2	9.5	6	6.6	7.5	6	6.5	8.2	7.6
Ho	0.9	1.4	1.4	1.4	1.7	1.1	1.1	1.3	1	1.1	1.4	1.2
Er	2.5	4.3	4	3.7	4.3	2.9	2.9	3.5	3	3.1	3.6	3.4
Tm	0.3	0.6	0.5	0.5	0.5	0.3	0.4	0.5	0.4	0.4	0.4	0.4
Yb	2.1	4.2	3.1	3.1	3.6	2.3	2.5	2.9	2.3	2.4	3.1	2.8
Lu	0.3	0.6	0.5	0.5	0.5	0.3	0.4	0.4	0.3	0.4	0.4	0.4
Th/Hf	1.41	0.90	1.27	2.03	1.24	1.81	1.47	1.88	1.11	1.55	1.81	2.95
La/Yb	28.86	17.14	22.19	21.26	21.17	19.09	17.72	18.48	18.43	28.58	18.13	25.86
Ce/Pb	22.00	12.30	33.16	31.58	27.87	26.58	44.29	37.24	25.47	22.13	34.84	20.97
Nb/U	37.89	26.19	46.00	35.56	35.26	37.73	50.17	38.60	39.00	23.46	38.33	18.97
Nb/Zr	0.29	0.16	0.29	0.20	0.16	0.24	0.26	0.25	0.27	0.19	0.24	0.26
Nb/Ba	0.19	0.15	0.36	0.34	0.47	0.10	0.13	0.13	0.12	0.06	0.12	0.06
La/Nb	0.57	0.58	0.93	1.16	1.14	0.78	0.74	0.93	0.68	1.22	0.98	1.23
Ce/Yb	57.62	36.90	40.65	38.71	36.39	38.13	37.20	37.24	37.65	56.25	34.84	53.93
La/Ta	11.02	22.50	12.91	16.56	15.97	11.37	9.93	13.11	10.34	17.32	14.79	17.66
Zr/Nb	3.40	6.43	3.42	4.97	6.34	4.15	3.92	3.94	3.77	5.35	4.16	3.84
Ba/Y	25.84	26.04	5.84	5.08	3.77	22.98	16.28	14.15	20.28	31.67	14.28	29.77
Zr/Hf	44.02	44.19	42.00	76.49	59.03	63.51	69.41	67.06	42.73	61.43	66.39	55.12
P2O5/TiO2	0.23	0.17	0.21	0.20	0.19	0.14	0.22	0.19	0.17	0.35	0.19	0.24

5. Discussion

5.1. Magma Compositions and Source Characteristics

Magma compositions of the studied rocks vary widely between maar products and

the coexisting rocks on the one hand, and between the two maars and the Njeu-Seh ejecta on the other hand. Considering the maar products solely, their Mg# varies between 0.31 - 0.54, and Ni and Cr contents are far below 250 ppm and 500 ppm, respectively, indicating that they are at most primary, but not primitive. They lack mantle xenoliths and xenocrysts, in contrast to most of the CVL maars spatters, but the crystal sizes suggest average to high ascent rates and a lack of storage in a magmatic chamber. The La/Ta ratios vary from 9.93 - 22.5 and 9.93 - 16.56 in the three maars pyroclasts. These La/Ta ratios are grossly indicative of an asthenospheric origin, based on the $22 < La/Ta \leq 30$ subdivisions of Coish & Sinton (1992). According to these authors, La/Ta ratios lower than 22 are typical of the asthenospheric mantle, while those between 22 - 30 characterize sub-continental lithospheric mantle, and values greater than 30 points to contaminated sources. Ce/Yb is also largely used to discriminate the depth and composition of the mantle source of rocks (Fitton et al., 1988; Leat et al., 1988; Thompson & Morrison, 1988; Coish & Sinton, 1992). The Manengouba Maars deposits show high Ce/Yb ratios (34.84 - 40.65) with respect to the barrier value of 20 considered as discriminative of asthenospheric spinel and garnet peridotites. The combination of La/Ta and Ce/Yb ratios suggests that the magma batch of the three Mount Manengouba Maars derived from an asthenospheric garnet peridotite and suffered only little or no crustal wall rock contamination.

5.2. Eruptive Dynamisms and Growth Models

The petrographic and geochemical data of samples from the Manengouba maars reveal fractional crystallization processes and complex interactions between magma and the surrounding rocks. The identified clinopyroxenes, plagioclases, olivines, and sanidines indicate a crystallization sequence where mafic minerals crystallized first, followed by felsic minerals. The presence of significant amounts of clinopyroxenes and plagioclases suggests crystallization at relatively high temperatures, typical of basic to intermediate magmas (Fitton & Dunlop, 1985). Positive Europium (Eu) anomalies observed in the samples indicate significant plagioclase crystallization under reducing conditions. These anomalies suggest that plagioclase incorporated Eu^{2+}, enriching the residual magma in Eu. This observation is consistent with intensive crystal fractionation, where plagioclase forms from the magmatic melt phase, altering the residual magma's chemical composition (Lorenz, 1986).

Recent studies on magmatic crystallization processes also show that interactions between crystallizing minerals and magmatic fluids can influence Eu anomalies. Brenna et al. (2021) highlight the importance of magmatic fluid dynamics in forming trace element anomalies and their distribution in volcanic rocks. Additionally, Ghasemi et al. (2019) demonstrated that pressure and temperature conditions during crystallization can significantly affect the partitioning of trace elements, including europium.

Mafic minerals (clinopyroxenes, olivines) crystallized first, indicating early-

stage high-temperature conditions. Felsic minerals (plagioclases, sanidines) crystallize later, reflecting a decrease in temperature and the evolution of the magma. Positive Eu anomalies in the samples suggest that plagioclase crystallized under reducing conditions, incorporating Eu^{2+} and enriching the residual magma. This process aligns with the crystal fractionation theory, where plagioclase significantly impacts the residual melt's composition. Magmatic fluid dynamics play a crucial role in forming and distributing trace element anomalies, as shown by Brenna et al. (2021). Interactions between crystallizing minerals and magmatic fluids can lead to varied trace element distributions and anomalies. The partitioning of trace elements, including Eu, is significantly affected by the crystallization conditions, such as pressure and temperature (Németh et al., 2003). These conditions influence the crystallization sequence and the resulting geochemical signatures in the rocks.

The combination of these factors provides a comprehensive understanding of the magmatic evolution in the Manengouba maars. The identified mineral phases, coupled with observed geochemical anomalies, highlight the intricate processes of fractional crystallization and the impact of magmatic fluid dynamics on trace element distribution. These insights are essential for interpreting the magmatic history and tectonic framework of the Manengouba region

5.2.1. Fractional Crystallization Processes and Their Impact on Mineral Composition

Petrographic and geochemical data from the Manengouba maars reveal complex fractional crystallization processes. The identified clinopyroxenes, plagioclases, olivines, and sanidines indicate a crystallization sequence in which mafic minerals crystallize first, followed by felsic minerals. Clinopyroxenes are present in varying percentages (20% - 35%), while plagioclases account for 19% - 35% of the samples, and olivines make up 5% - 15%. This crystallization sequence is typical of basic to intermediate magmas, where high crystallization temperatures favor the initial formation of mafic minerals (Fitton & Dunlop, 1985).

Positive Europium (Eu) anomalies observed in the samples suggest significant plagioclase crystallization under reducing conditions. These anomalies indicate that plagioclase incorporated Eu^{2+}, thereby enriching the residual magma in Eu. This observation is consistent with intensive crystal fractionation, where plagioclase forms from the magmatic melt phase, altering the residual magma's chemical composition (Lorenz, 1986).

5.2.2. Role of Deep Magmatic Sources in Magma Evolution

Deep magmatic sources play a crucial role in the evolution of magmas in the Manengouba region. Geochemical analyses show enrichments in trace elements such as Nb (10 to 50 ppm) and Zr (up to 200 ppm), indicating contributions from enriched mantle sources. Recent studies by Brenna et al. (2021) and Blundy et al. (2010) emphasize the importance of interactions between magma and deep mantle sources in magmatic differentiation and the formation of trace element anom-

alies. The high-temperature crystallization favors mafic mineral formation, typical of basic to intermediate magmas. Positive Eu anomalies indicate significant plagioclase crystallization under reducing conditions. Incorporation of Eu^{2+} into plagioclase enriches the residual magma in Eu, reflecting intensive crystal fractionation processes. Enrichments in Nb and Zr suggest contributions from enriched mantle sources. Interactions with deep mantle sources are crucial for magmatic differentiation and trace element anomaly formation. Deep mantle sources contribute to the enriched trace element profiles seen in the magmas. These interactions are key to understanding the magmatic evolution and the formation of specific geochemical signatures in the Manengouba maars region.

These insights into fractional crystallization processes and the role of deep magmatic sources provide a comprehensive understanding of the magmatic evolution in the Manengouba maars. The identified mineral phases and geochemical anomalies highlight the intricate processes that shape the region's magmatic history.

5.3. Geochemical Correlations

The correlations between major elements and trace elements in the rocks from the Manengouba maars reveal significant geochemical processes. Strong positive correlations between SiO_2 and light rare earth elements (LREE) such as La (0.748), Ce (0.750), and Nd (0.671) indicate an enrichment of LREE in SiO_2-rich rocks. This suggests advanced magmatic differentiation, where these elements are concentrated in residual liquids, typical of evolved magmas. For Al_2O_3, significant correlations with Sr (0.540) and Zr (0.562) indicate that Sr is mainly incorporated into plagioclase, reflecting significant crystallization of these minerals. The correlations with Zr and Hf (0.511) suggest the presence of zircon and other accessory minerals, indicating advanced magmatic differentiation.

Strong positive correlations between Fe_2O_3 and compatible elements such as Co (0.852), Ni (0.819), and Cr (0.735) indicate significant crystallization of mafic minerals like pyroxenes and olivines, reflecting the ultramafic nature of the magmas and early fractionation of these minerals. Similarly, the correlations between MgO and Co (0.800), Ni (0.704), and Cr (0.679) confirm the crystallization of mafic minerals, with a positive correlation between MgO and V (0.833) suggesting significant incorporation of vanadium into spinels. Lastly, correlations between Na_2O and Rb (0.794) as well as K_2O and Ba (0.770) indicate an association with alkali feldspars, suggesting late-stage crystallization of these minerals in evolved magmas. These observations show that alkali feldspars play a crucial role in the late-stage crystallization of magmas, indicating complex differentiation and crystallization processes in the rocks from the Manengouba maars.

Positive correlations indicate advanced magmatic differentiation, where incompatible elements are enriched in residual liquids. This is typical of evolved magmas, where incompatible elements are retained in the magmatic liquid longer during fractional crystallization. SiO_2-rich rocks thus have higher concentrations of LREE, suggesting advanced magmatic evolution. Strong positive correlations

confirm that plagioclase is a significant mineral phase in the studied rocks. Sr is compatible with plagioclase, suggesting significant crystallization of this mineral. Positive correlations with Zr and Hf indicate the presence of accessory minerals such as zircon, typical of evolved magmas. Correlations indicate significant crystallization of mafic minerals, mainly pyroxenes and olivines. These minerals incorporate these trace elements, enriching the rocks in Fe_2O_3 and MgO. This suggests that magmatic fractionation processes in these rocks involve early separation of mafic phases, enriching the residual magma in incompatible elements. Correlations between certain trace elements (such as Zn and Mo) and major elements may indicate interactions with hydrothermal fluids. For example, a moderate correlation between Fe_2O_3 and Zn suggests that zinc-bearing metallic minerals may have formed or been altered by hydrothermal fluids. These interactions can also contribute to the enrichment or depletion of certain elements in the volcanic rocks studied.

The analyses of correlations between major and trace elements provide crucial information on the magmatic and tectonic processes that led to the formation of volcanic rocks in the Manengouba maars region. The enrichment in incompatible elements and correlations with compatible elements suggest phases of fractional crystallization and complex interactions between magmas and mineral phases.

5.4. Hydrothermal Alteration: Impact of Hydrothermal Fluids on Mineral Composition

Signs of hydrothermal alteration observed in clinopyroxenes and olivines, notably the transformation of olivine into serpentine, indicate post-crystallization interaction with hydrothermal fluids. These interactions modify the mineral composition of the rocks, affecting the physical properties of the pyroclastic deposits. X-ray diffraction (XRD) analyses reveal a significant presence of smectite (25.99% - 76.05%) and kaolinite, indicating extensive hydrothermal alteration. Studies by Gouy et al. (2023) show that hydrothermal alteration is often linked to local tectonic activity, influencing the distribution and composition of clay minerals.

Hydrothermal alteration signs observed in clinopyroxenes and olivines, such as the transformation of olivine into serpentine, suggest post-crystallization interaction with hydrothermal fluids. These interactions can modify the mineral composition of the rocks and affect the physical properties of the pyroclastic deposits. Opaque mineral inclusions, such as magnetite and ilmenite, suggest fluctuating oxidation conditions during and after magma crystallization (White & Ross, 2011). X-ray diffraction (XRD) analyses show a significant presence of smectite, kaolinite, and other clay minerals, indicating extensive hydrothermal alteration. These clay minerals typically form under moderate temperature and pressure conditions, characteristic of hydrothermal environments associated with active volcanic systems. Recent studies, such as those by Gouy et al. (2023), have shown that hydrothermal alteration in volcanic environments can be closely related to local tectonic activity, influencing the distribution and composition of clay minerals.

Lerouge et al. (2023) have also highlighted the importance of hydrothermal fluid circulation in modifying the isotopic and geochemical signatures of altered volcanic rocks.

Transformation of olivine into serpentine and alteration of clinopyroxenes indicate interaction with hydrothermal fluids. These interactions modify the mineral composition and affect the physical properties of pyroclastic deposits. The significant presence of smectite (25.99% to 76.05%) and kaolinite indicates extensive hydrothermal alteration. These minerals form under moderate temperature and pressure conditions typical of hydrothermal environments. Hydrothermal alteration is often linked to local tectonic activity, influencing the distribution and composition of clay minerals (Gouy et al., 2023). Studies highlight the importance of hydrothermal fluid circulation in altering the isotopic and geochemical signatures of volcanic rocks (Lerouge et al., 2023). The presence of magnetite and ilmenite suggests fluctuating oxidation conditions during and after magma crystallization. These conditions affect the mineralogical composition and the geochemical signatures of the rocks.

These findings provide a comprehensive understanding of the impact of hydrothermal fluids on the mineral composition of the Manengouba maars. The extensive hydrothermal alteration and its link to tectonic activity highlight the complex interactions between magmatic processes and post-crystallization fluid dynamics.

5.5. Interactions between Magma and Country Rocks

Interactions between magma and country rocks play a crucial role in the evolution of pyroclastic deposits. Opaque mineral inclusions such as magnetite and ilmenite suggest fluctuating oxidation conditions during and after magma crystallization. These interactions alter the chemical composition of the magmas, enriching them in trace elements and rare earth elements (REE) (White & Ross, 2011). Studies by Lerouge et al. (2023) emphasize the importance of hydrothermal fluid circulation in modifying the isotopic and geochemical signatures of altered volcanic rocks. The presence of these hydrothermal fluids and their interactions with both the magma and the surrounding rocks lead to significant changes in mineral composition and trace element distribution.

Opaque mineral inclusions such as magnetite and ilmenite indicate varying oxidation conditions during and after crystallization. These conditions influence the chemical composition of the magmas. Interactions between magma and country rocks result in the enrichment of magmas in trace elements and REE. These chemical changes are crucial for understanding the evolution of pyroclastic deposits. Hydrothermal fluids play a significant role in modifying the isotopic and geochemical signatures of volcanic rocks. These fluids interact with the magma and surrounding rocks, leading to changes in mineral composition and trace element distribution. The interaction between magma and country rocks affects the physical and chemical properties of pyroclastic deposits. Understanding these interactions is essential for interpreting the magmatic and tectonic history of the region.

These interactions highlight the complex processes involved in the evolution of magmas and their impact on the surrounding geological environment. The enrichment in trace elements and REE, along with the influence of hydrothermal fluids, provides valuable insights into the magmatic processes and post-crystallization modifications in the Manengouba maars.

6. Conclusion

This in-depth study of the maars of Manengouba, located along the Cameroon Volcanic Line (CVL), reveals a complex magmatic evolution marked by processes of fractional crystallization, hydrothermal alteration, and dynamic interactions between magma and country rocks. Petrographic data show a diverse mineralogical composition with a crystallization sequence in which mafic minerals crystallize first, followed by felsic minerals. The Europium (Eu) anomalies observed in the samples suggest crystallization under reducing conditions, consistent with intensive fractional crystallization.

Geochemical analyses reveal clear trends of magmatic fractionation, indicating that the magmas underwent significant differentiation before eruption. Explosive interactions between ascending magma and groundwater led to phreatomagmatic explosions, forming complex diatreme structures. The presence of mantle xenoliths and fragments of country rock in the breccias indicates significant assimilation of country rocks during magma ascent, altering their chemical composition.

Hydrothermal alteration, confirmed by XRD analyses, shows post-crystallization transformation of minerals, indicating interactions with hydrothermal fluids. These alterations have modified the mineralogical composition of the rocks, influencing the physical properties of the pyroclastic deposits.

The results of this study propose a detailed model of diatreme growth in the Manengouba region, highlighting the importance of phreatomagmatic interactions and magmatic fractionation processes. Compared to other volcanic regions, the geology of Manengouba shows significant similarities with other volcanoes along the CVL, as well as with maars and diatremes studied elsewhere in the world.

Declaration of Interest statement

The authors declare that they have no known competing financial interests or personal relationships that could have appeared to influence the work reported in this paper.

Conflicts of Interest

The authors declare no conflicts of interest regarding the publication of this paper.

References

Blundy, J., Cashman, K. V., Rust, A., & Witham, F. (2010). A Case for CO_2-Rich Arc Magmas. *Earth and Planetary Science Letters, 290,* 289-301.

https://doi.org/10.1016/j.epsl.2009.12.013

Boggs Jr., S. (2009). *Petrology of Sedimentary Rocks* (612 p.). Cambridge University Press. https://doi.org/10.1017/cbo9780511626487

Branney, M. J., & Kokelaar, B. P. (2002). *Pyroclastic Density Currents and the Sedimentation of Ignimbrites*. The Geological Society of London.

Brenna, M., Cronin, S. J., Smith, I. E. M., Sohn, Y. K., & Németh, K. (2010). Mechanisms Driving Polymagmatic Activity at a Monogenetic Volcano, Udo, Jeju Island, South Korea. *Contributions to Mineralogy and Petrology, 160,* 931-950. https://doi.org/10.1007/s00410-010-0515-1

Brenna, M., Ubide, T., Nichols, A. R., Mollo, S., & Pontesilli, A. (2021). Anatomy of Intraplate Monogenetic Alkaline Basaltic Magmatism: Clues from Magma, Crystals, and Glass. In *Crustal Magmatic System Evolution: Anatomy, Architecture, and Physicochemical Processes* (pp. 79-103). American Geophysical Union.

Chako Tchamabé, B., Ohba, T. I., Ooki, S., Youmen, D., Owona, S. et al. (2014). Temporal Evolution of the Barombi Mbo Maar, a Polygenetic Maar-Diatreme Volcano of the Cameroon Volcanic Line. *International Journal of Geosciences, 5,* 1315-1323. https://doi.org/10.4236/ijg.2014.511108

Chako-Tchamabé, B., Graettinger, A., Gountié Dedzo, M., Tamen, J., Nemeth, K., Weber, B. et al. (2023). Influence of Deep Magmatic Source Region in the Growth of Complex Maar-Diatreme Volcanoes. *Geological Journal, 59,* 680-700. https://doi.org/10.1002/gj.4887

Coish, R. A., & Sinton, C. W. (1992). Geochemistry of Mafic Dikes in the Adirondack Mountains: Implications for Late Proterozoic Continental Rifting. *Contributions to Mineralogy and Petrology, 110,* 500-514. https://doi.org/10.1007/bf00344084

Fitton, J. G., & Dunlop, H. M. (1985). The Cameroon Line, West Africa, and Its Bearing on the Origin of Oceanic and Continental Alkali Basalt. *Earth and Planetary Science Letters, 72,* 23-38. https://doi.org/10.1016/0012-821x(85)90114-1

Fitton, J. G., James, D., Kempton, P. D., Ormerod, D. S., & Leeman, W. P. (1988). The Role of Lithospheric Mantle in the Generation of Late Cenozoic Basic Magmas in the Western United States. *Journal of Petrology, Special_Volume,* 331-349. https://doi.org/10.1093/petrology/special_volume.1.331

Floyd, P. A., & Winchester, J. A. (1977). Geochemical Discrimination of Different Magma Series and Their Differentiation Products Using Immobile Elements. *Chemical Geology, 20,* 325-343. https://doi.org/10.1016/0009-2541(77)90057-2

Ghasemi, H., Kazemi, Z., Mousivand, F., & Grifn, W. (2018). Whole-Rock Geochemistry and Mineral Chemistry of the Late Cretaceous Dacites in SW Sabzevar: Constrain on Their Origin and Tectonic Setting. *Petrology, 9,* 79-100.

Gouy, M., Tannier, E., Comte, N., & Parsons, D. P. (2023). Seaview Version 5: A Multiplatform Software for Multiple Sequence Alignment, Molecular Phylogenetic Analyses, and Tree Reconciliation. In K. Katoh (Ed.), *Multiple Sequence Alignment* (pp. 241-260). Springer US. https://doi.org/10.1007/978-1-0716-1036-7_15

Indriyanto, J. N., Ohba, T., Hoshide, T., Angkasa, S. S., & Abdurrachman, M. (2023). Eruptive History of the Last-1300-Years Activity of Kelud Volcano, Indonesia: Inferences from Stratigraphy, Chronology, Sedimentology, Componentry, and Geochemistry. *Journal of Volcanology and Geothermal Research, 433,* Article ID: 107723. https://doi.org/10.1016/j.jvolgeores.2022.107723

Ishikawa, Y., Sawaguchi, T., Iwaya, S., & Horiuchi, M. (1976). Delineation of Prospecting Targets for Kuroko Deposits Based on Modes of Volcanism of Underlying Dacite and Alteration Haloes. *Mining Geology, 26,* 105-117.

Kagou Dongmo, A., Wandji, P., Pouclet, A., Vicat, J., Cheilletz, A., Nkouathio, D. G. et al. (2001). Évolution volcanologique du mont Manengouba (Ligne du Cameroun); nouvelles données pétrographiques, géochimiques et géochronologiques. *Comptes Rendus de l'Académie des Sciences-Series IIA-Earth and Planetary Science, 333,* 155-162. https://doi.org/10.1016/s1251-8050(01)01625-1

Kagou Dongmo, A., Nkouathio, D., Pouclet, A., Bardintzeff, J., Wandji, P., Nono, A. et al. (2010). The Discovery of Late Quaternary Basalt on Mount Bambouto: Implications for Recent Widespread Volcanic Activity in the Southern Cameroon Line. *Journal of African Earth Sciences, 57,* 96-108. https://doi.org/10.1016/j.jafrearsci.2009.07.015

Kereszturi, G., Németh, K., Cronin, S. J., Agustín-Flores, J., Smith, I. E. M., & Lindsay, J. (2013). A Model for Calculating Eruptive Volumes for Monogenetic Volcanoes—Implication for the Quaternary Auckland Volcanic Field, New Zealand. *Journal of Volcanology and Geothermal Research, 266,* 16-33. https://doi.org/10.1016/j.jvolgeores.2013.09.003

Kurszlaukis, S., & Fulop, A. (2013). Factors Controlling the Internal Facies Architecture of Maar-Diatreme Volcanoes. *Bulletin of Volcanology, 75,* Article No. 761. https://doi.org/10.1007/s00445-013-0761-y

Large, R. R., Allen, R. L., Blake, M. D., & Herrmann, W. (2001). Hydrothermal Alteration and Volatile Element Halos for the Rosebery K Lens Volcanic-Hosted Massive Sulfide Deposit, Western Tasmania. *Economic Geology, 96,* 1055-1072. https://doi.org/10.2113/gsecongeo.96.5.1055

Le Bas, M. J., Maitre, R. W. L., Streckeisen, A., & Zanettin, B. (1986). A Chemical Classification of Volcanic Rocks Based on the Total Alkali-Silica Diagram. *Journal of Petrology, 27,* 745-750. https://doi.org/10.1093/petrology/27.3.745

Leat, P. T., Thompson, R. N., Morrison, M. A., Hendry, G. L., & Dickin, A. P. (1988). Compositionally-Diverse Miocene—Recent Rift-Related Magmatism in Northwest Colorado: Partial Melting, and Mixing of Mafic Magmas from 3 Different Asthenospheric and Lithospheric Mantle Sources. *Journal of Petrology, Special_Volume,* 351-377. https://doi.org/10.1093/petrology/special_volume.1.351

Lentz, D. R. (1996). *Recent Advances in Lithogeochemical Exploration for Massive Sulphide Deposits in Volcano-Sedimentary Environments: Petrogenetic, Chemostratigraphic and Alteration Aspects with Examples from the Bathurst Camp, New Brunswick* (pp. 73-119). New Brunswick Department of Natural Resources and Energy, Mineral and Energy Division Mineral Resources Report 961.

Lentz, D. R. (1999). Petrology, Geochemistry, and Oxygen Isotope Interpretation of Felsic Volcanic and Related Rocks Hosting the Brunswick 6 and 12 Massive Sulfide Deposits (Brunswick Belt), Bathurst Mining Camp, New Brunswick, Canada. *Economic Geology, 94,* 57-86. https://doi.org/10.2113/gsecongeo.94.1.57

Lerouge, C., Debure, M., Fernández, A., Négrel, P., Madé, B., Maubec, N. et al. (2023). Hydrogeochemical Processes of Critical Zone Developed in Tégulines Clay, Paris Basin: Hydrogeochemical and Multi-Isotopic Approach (δ13C, δD, δ18O, 87Sr/86Sr and 14C). *Journal of Hydrology, 617,* Article ID: 129077. https://doi.org/10.1016/j.jhydrol.2023.129077

Lorenz, V. (1986). On the Growth of Maars and Diatremes and Its Relevance to the Formation of Tuff Rings. *Bulletin of Volcanology, 48,* 265-274. https://doi.org/10.1007/bf01081755

Makishima, A., & Nakamura, E. (1997). Suppression of Matrix Effects in ICP-MS by High Power Operation of ICP: Application to Precise Determination of Rb, Sr, Y, Cs, Ba, REE, Pb, Th and U at Ng G^{-1} Levels in Milligram Silicate Samples. *Geostandards Newsletter, 21,* 307-319. https://doi.org/10.1111/j.1751-908x.1997.tb00678.x

McDonough, W. F., & Sun, S. (1995). The Composition of the Earth. *Chemical Geology, 120,* 223-253. https://doi.org/10.1016/0009-2541(94)00140-4

Németh, K., White, J. D. L., Reay, A., & Martin, U. (2003). Compositional Variation during Monogenetic Volcano Growth and Its Implications for Magma Supply to Continental Volcanic Fields. *Journal of the Geological Society, 160,* 523-530. https://doi.org/10.1144/0016-764902-131

Ngounouno, I., Déruelle, B., Guiraud, R., & Vicat, J. (2001). Magmatismes tholéiitique et alcalin des demi-grabens crétacés de Mayo Oulo-Léré et de Babouri–Figuil (Nord du Cameroun-Sud du Tchad) en domaine d'extension continentale. *Comptes Rendus de l'Académie des Sciences-Series IIA-Earth and Planetary Science, 333,* 201-207. https://doi.org/10.1016/s1251-8050(01)01626-3

Pearce, J.A. (1996). A User's Guide to Basalt Discrimination Diagrams. In D. A. Wyman (Ed.), *Trace Element Geochemistry of Volcanic Rocks: Applications for Massive Sulphide Exploration* (Vol. 12, pp. 79-113). Geological Association of Canada, Short Course Notes.

Pedrazzi, D., Martí, J., & Geyer, A. (2013). Stratigraphy, Sedimentology and Eruptive Mechanisms in the Tuff Cone of El Golfo (Lanzarote, Canary Islands). *Bulletin of Volcanology, 75,* Article No. 740. https://doi.org/10.1007/s00445-013-0740-3

Pouclet, A., Kagou Dongmo, A., Bardintzeff, J., Wandji, P., Chakam Tagheu, P., Nkouathio, D. et al. (2014). The Mount Manengouba, a Complex Volcano of the Cameroon Line: Volcanic History, Petrological and Geochemical Features. *Journal of African Earth Sciences, 97,* 297-321. https://doi.org/10.1016/j.jafrearsci.2014.04.023

Tchoua, M. F. (1974). *Contribution à l'étude géologique et pétrographique de quelques volcans de la Ligne du Cameroun. (Monts Manengouba et Bambouto)* (p. 337). Thèse Doct. Etat, Univ. Clermont-Ferrand.

Thompson, R. N., & Morrison, M. A. (1988). Asthenospheric and Lower-Lithospheric Mantle Contributions to Continental Extensional Magmatism: An Example from the British Tertiary Province. *Chemical Geology, 68,* 1-15. https://doi.org/10.1016/0009-2541(88)90082-4

White, J. D. L., & Ross, P. S. (2011). Maar-Diatreme Volcanoes: A Review. *Journal of Volcanology and Geothermal Research, 201,* 1-29.

Zangmo Tefogoum, G., Kagou Dongmo, A., Nkouathio, D. G., & Gountié Dedzo, M. (2021). Highlight of Geotouristic Values of a Volcanic Landform on the Mount Manengouba Eastern Slopes: Case of Djeu-Seh Basin. In R. B. Singh, D. Y. Wei, & S. Anand (Eds.), *Global Geographical Heritage, Geoparks and Geotourism* (pp. 407-426). Springer. https://doi.org/10.1007/978-981-15-4956-4_21